NCAT Report 06-04

Forensic Investigation of a Rich-Bottom Pavement

By

J. Richard Willis
David H. Timm

December 2006

FORENSIC INVESTIGATION OF A RICH-BOTTOM PAVEMENT

by

J. Richard Willis, Graduate Research Assistant
David H. Timm, PhD, P.E., Gottlieb Associate Professor of Civil Engineering
National Center for Asphalt Technology
Auburn University, Alabama

NCAT Report 06-04

December 2006

"The contents of this report reflect the views of the authors who are solely responsible for the facts and the accuracy of the data presented herein. The contents do not necessarily reflect the official view and policies of the National Center for Asphalt Technology of Auburn University. This report does not constitute a standard, specification, or regulation."

ACKNOWLEDGEMENTS

The authors wish to thank the National Asphalt Pavement Association for sponsoring this forensic investigation. The Alabama Department of Transportation, the Indiana Department of Transportation and the Federal Highway Administration also deserve special recognition for their support and cooperation with the Structural Study at the Test Track. Special thanks to Buzz Powell, Jennifer Still, Blake Lockhart and Charles Godwin for their assistance.

TABLE OF CONTENTS

LIST OF TABLES

LIST OF FIGURES

CHAPTER 1 - INTRODUCTION

BACKGROUND

Since the inception of pavement design processes, engineers have been searching for ways to increase the life of their structures. Not only would a stronger and longer-lasting pavement be more economical for its owner, but it would also reduce the ever growing dilemma of congestion on highways due to rehabilitation services being performed on the structure. With reduced rehabilitation comes a reduced delay on the structure's users. From these needs has arisen the idea of creating a perpetual pavement.

The Asphalt Pavement Alliance (APA, 2002) defined a perpetual pavement as "an asphalt pavement designed and built to last longer than 50 years without requiring major structural rehabilitation or reconstruction, and needing only periodic surface renewal in response to distresses confined to the top of the pavement."

Newcomb *et al.* (2001) described a basic structure that could qualify as a perpetual pavement. This pavement involved combining "a rut resistant, impermeable, and wear resistant top structural layer with a rut resistant and durable intermediate layer and a fatigue resistant and durable base layer." This structure is illustrated in Figure 1.1.

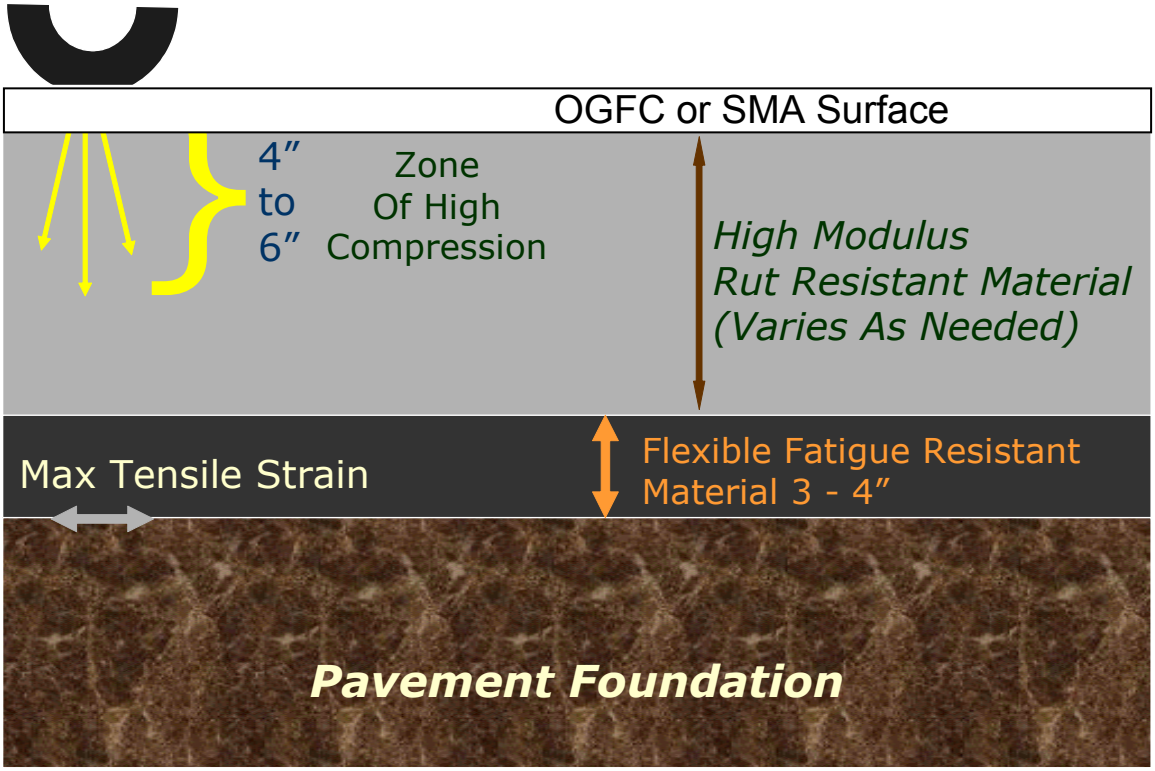

Figure 1.1 Perpetual Pavement Design Concept (Newcomb *et al.*, 2001).

In order for a pavement to be perpetual, the resistance to fatigue cracking must be maximized. This is done by decreasing the amount of tensile strain in the pavement while keeping the structure simple and constructible (Harvey *et al.*, 2004). While SMA

and other mixtures are used to help create the rut resistant and impermeable top layer, the base layer of the hot mix asphalt (HMA) has to withstand the tendency to crack due to fatigue. To help endure the tensile strains at the bottom of HMA, it has been stated (Newcomb *et al*., 2001), "The main mixture characteristic which can help guard against fatigue cracking is a higher asphalt content."

Increasing the asphalt content in the bottom layer of HMA is commonly referred to as a rich-bottom. In 2002, both California and Illinois had used this type of structure and seen positive results (Harm, 2001; APA, 2002). The addition of asphalt to the base HMA layer has seen three positive results.
1) Additional asphalt improves moisture damage resistance
2) Additional asphalt increases fatigue life
3) Additional asphalt allows for easier placement and compaction during construction.
While these three benefits have been seen (Harm, 2001), the increase in fatigue life is the primary concern of this report.

The increase in asphalt content helps increase the fatigue life of the pavement through better compaction, meaning lower air voids, which improves the pavement's fatigue resistance (St. Martin *et al*., 2001). "The purpose of increased asphalt content is to facilitate compaction to the range of zero to three percent [air voids] in the field" (Harvey *et al.*, 2004).

Laboratory tests have been conducted showing the effect asphalt content and air voids have on fatigue resistance, and the compaction level has been shown to have a larger impact than asphalt content. Although, it should be recognized that asphalt and air content are interdependent variables and that increasing asphalt contents will generally result in lower air voids (Harvey *et al.*, 2004).

Research has been conducted within the past few years to determine the needs and limitations of pavement structures including rich-bottom layers. Owners would still like to have the pavements as thin as possible to help reduce initial costs so research has been conducted to determine location (i.e., depth below overlying layers) and thickness of the rich-bottom layer. Today, it is recommended that rich-bottom pavements be built with a 0.5% increase in asphalt in the bottom lift that is between 2 to 3 inches in thickness. Thickness beyond three inches proved to have insignificant benefits to the fatigue life of the structure. Further, the rich-bottom layer should be at least 6 inches below the surface to protect it from possible damage due to its lack of shear resistance (Harvey *et al.*, 2004).

Another technique some have used to facilitate the design of the rich-bottom layer is to design the mix for lower air voids. This methodology was implemented in the design of the rich-bottom layers for Oklahoma in the 2006 Test Track cycle.

NCAT TEST TRACK AND SECTION N8

In 2003, the National Center for Asphalt Technology (NCAT) rebuilt the original 1.7 mile Test Track, seen in Figure 1.2, in Opelika, Alabama. The track is an accelerated loading facility where the pavement is subjected to approximately 10 million ESALs in two and a half years. Included in this new study were eight 200 ft structural test sections to investigate mechanistic-empirical pavement design and analysis concepts. All eight sections were built upon an improved roadbed and 6 inches of crushed aggregate base course. The differences in the 8 sections were the thicknesses and designs of the HMA layers as indicated in Figure 1.3.

Figure 1.2 NCAT Test Track.

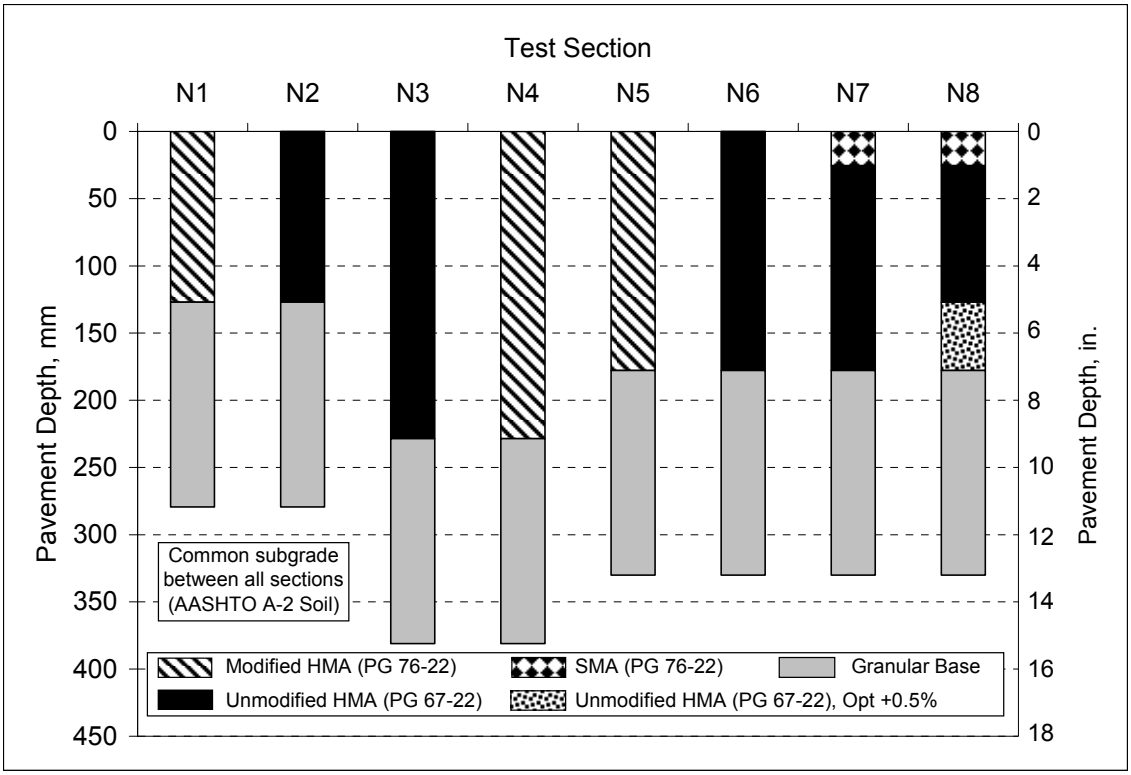

Figure 1.3 Structural Study Cross Sections (Priest and Timm, 2005).

Sections N7 and N8 are the two sections of particular interest to this report due to their similarities. As can be seen, each HMA layer was 7 inches thick comprised of a 1 inch SMA layer at the top of the pavement. The only difference in the two sections was the 2 inch rich bottom layer as the bottom lift in N8 where the additional asphalt decreased total air voids by almost 2 percent. Figure 1.4 and Table 1.1 give properties for the mixes used in the construction of N7 and N8. In both of these sections, strain gauges were built into the pavement structure at the bottom and on top of lift four.

Tack coats were applied between all pavement lifts. PG 67-22 binder was used as the tack and applied at a target rate of 0.03 gallons per square yard. This tack application was used for both sections.

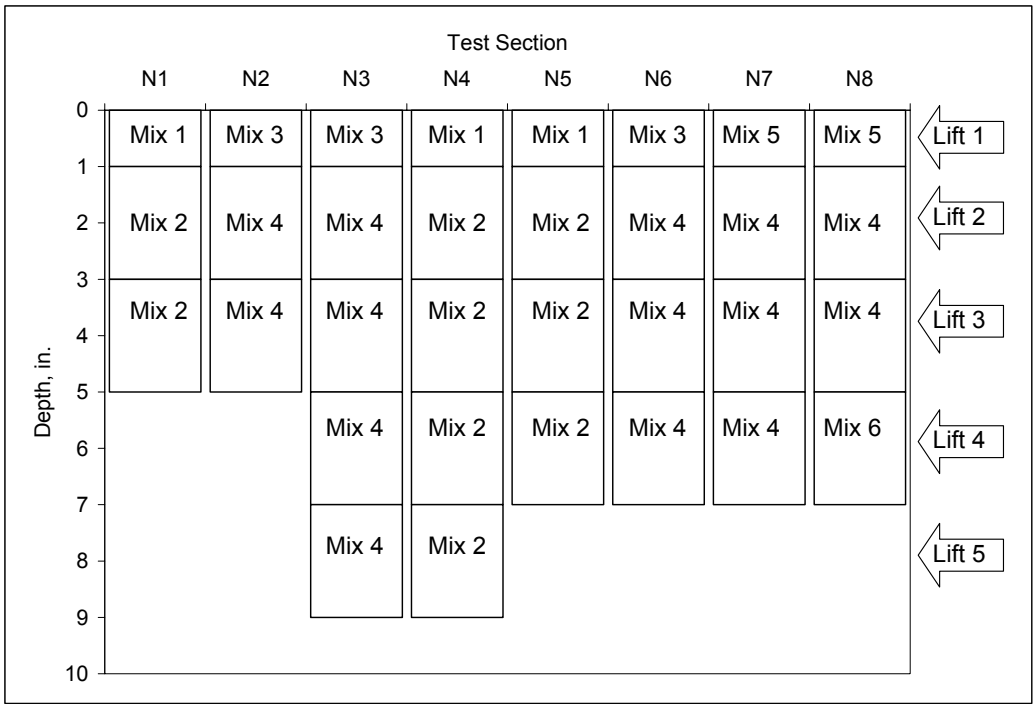

Figure 1.4 HMA Sublayer Mixture Numbering (Timm and Priest, 2006).

Table 1.1 HMA Mix Design Parameters (Timm and Priest, 2006)

Asphalt Mixture	1	2	3	4	5	6
Asphalt PG Grade	76-22	76-22	67-22	67-22	76-22	67-22
Gradation	Wearing	Base	Wearing	Base	SMA	Base
Liquid Antistrip Agent, %	0.5	None	0.5	None	None	None
Design Methodology	Super	Super	Super	Super	Marshall	Super
Compaction Device	Gyratory	Gyratory	Gyratory	Gyratory	Hammer	Gyratory
Compactive Effort, Number of Gyrations	80	80	80	80	50	80
Mixing Temperature, F	345	345	325	325	345	325
Effective Asphalt Content, %	6.13	4.27	6.13	4.27	6.05	4.77
Dust to Asphalt Ratio	0.88	1.10	0.88	1.10	1.50	0.99
Maximum Specific Gravity of Mix	2.474	2.571	2.474	2.571	2.447	2.536
Effective Specific Gravity of Aggregate Blend	2.729	2.766	2.729	2.766	2.687	2.747
Bulk Unit Weight of Compacted Pills, pcf	147.8	153.6	147.8	153.6	145.9	155.5
Tensile Strength Ratio	0.83	0.83	0.83	0.83	0.87	Unknown
Computed Air Voids in Total Mix, %	4.3	4.3	4.3	4.3	4.1	2.5
Voids in Mineral Aggregate, %	17.9	14.5	17.9	14.5	17.9	13.5

N8 was originally designed to withstand a loading cycle of 7 million ESALs with a rich bottom layer. The purpose of this experiment was to determine if the rich bottom would help improve the performance of the section in the accelerated load testing conditions. However, N8 was soon found to perform poorly relative to the other 7 in. sections.

On August 2, 2004, a surface distress survey found that 0.69% of N8 was showing fatigue cracking. In comparison, N7 showed 0.05% cracking three months later. Not only was this the case, but a rapid deterioration of section N8 continued. This brought many questions and concerns to the minds of those associated with the track. Was the

rich bottom layer the cause of accelerated fatigue cracking, or could another explanation be found as to why the phenomenon occurred?

It was hypothesized that the structural fatigue damage was due to a possible debonding in the pavement. The high level of fatigue was a fairly localized phenomenon; therefore, a widespread mix flaw was not suspected as causing the deterioration.

OBJECTIVES

The objective of this study was to forensically and theoretically investigate the cause of fatigue damage in the rich bottom test section. Specifically, three questions were to be answered in relation to the theory of debonding.

1. Do the dynamic strain data support the idea of slippage occurring?
2. Can any physical evidence be found in the pavement structure to point to debonding of layers?
3. Are the interface bond strengths in N8 comparable to those of the similarly constructed N7?

SCOPE

The work for this project was completed in three phases. First, a careful study of the dynamic strain data was completed comparing the strains of N8 to those of N7. Ratios were then taken of the strains measured in the top lift, 2 inches above the base layer, to those at the base/HMA interface for both Sections N7 and N8. These were subsequently compared to theoretical values calculated through the WESLEA for Windows linear elastic analysis program. Secondly, trenches were cut into the pavement structure to find physical evidence of any cracking or debonding in the section. Finally, cores were cut from specific portions of N8 and N7 to compare bond strengths between the two sections.

CHAPTER 2 - DYNAMIC STRAIN STUDY

STRAIN DATA

The 2003 NCAT Test Track was an accelerated loading facility containing eight instrumented sections to study the structural effects of loading the pavement. N7 and N8 were both instrumented as show in Figures 2.1 through 2.3. Both N7 and N8 had a set of 12 strain gauges centered symmetrically about the outside wheelpath, where most of the deterioration occurred in N8. N8 also had an extra set of 8 strain gauges set up along the inside wheelpath to make inside vs. outside wheelpath comparisons.

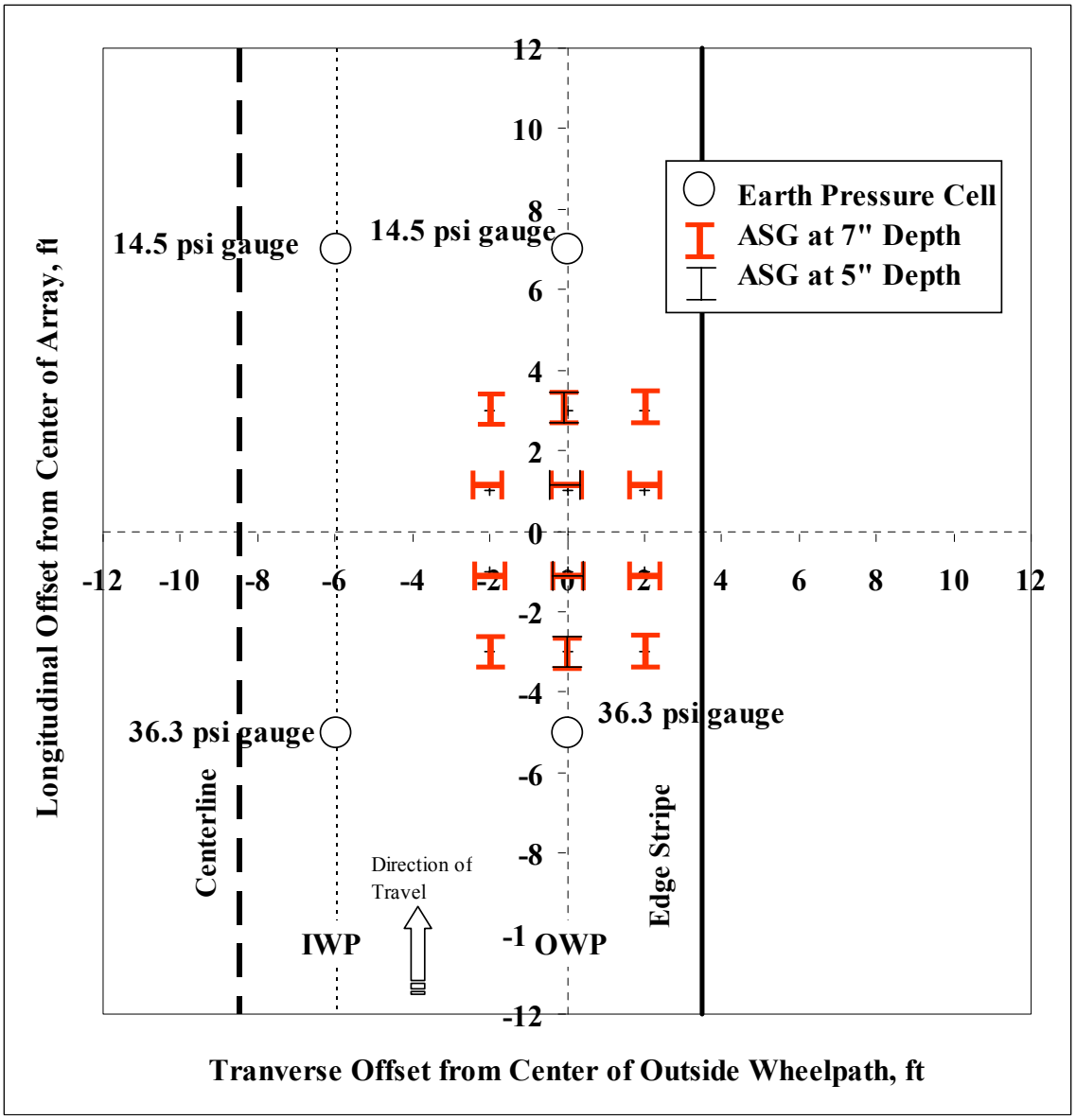

Figure 2.1 N7 Gauge Arrangement (Timm *et al.*, 2004).

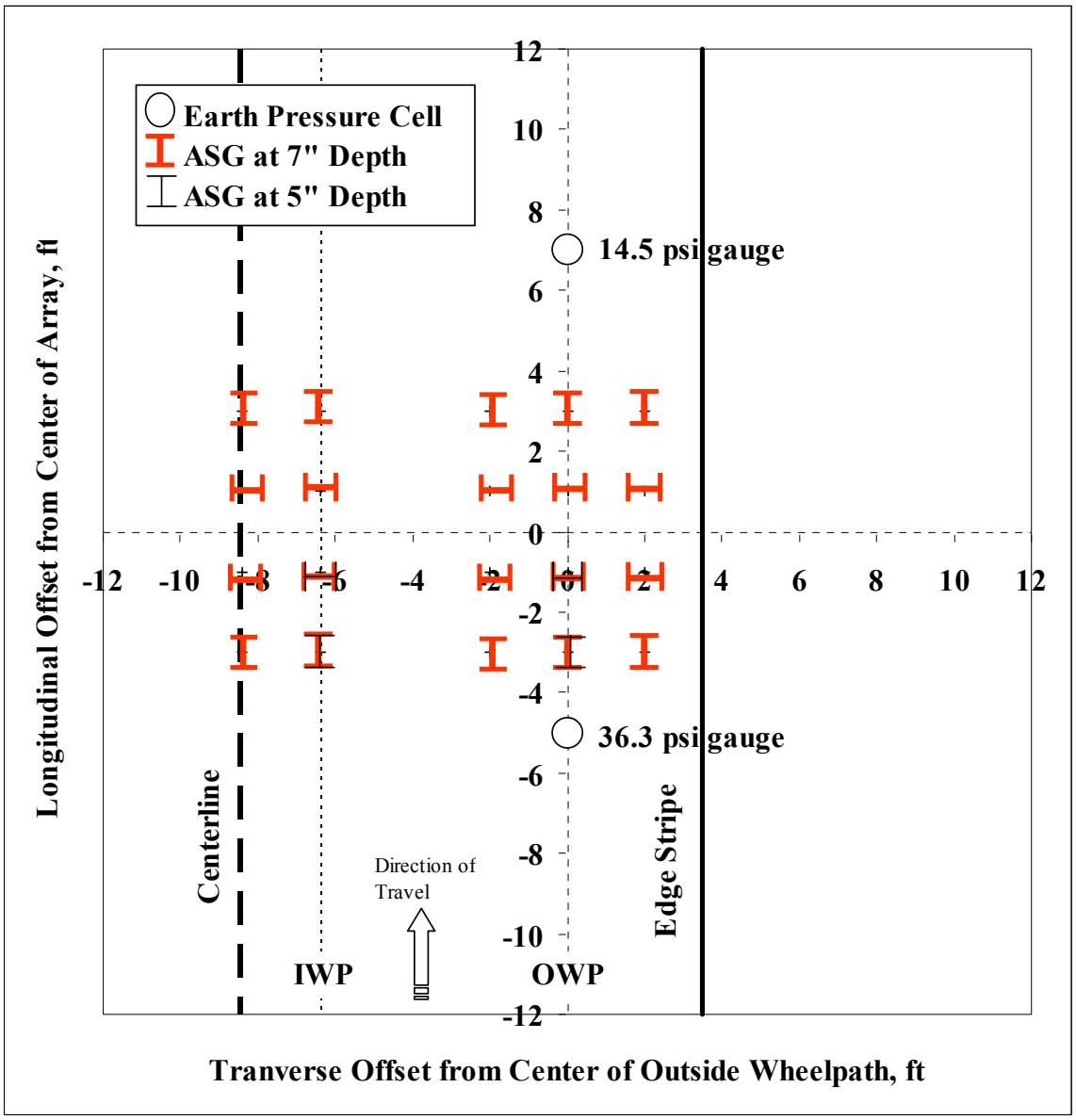

Figure 2.2 N8 Gauge Arrangement (Timm *et al.*, 2004).

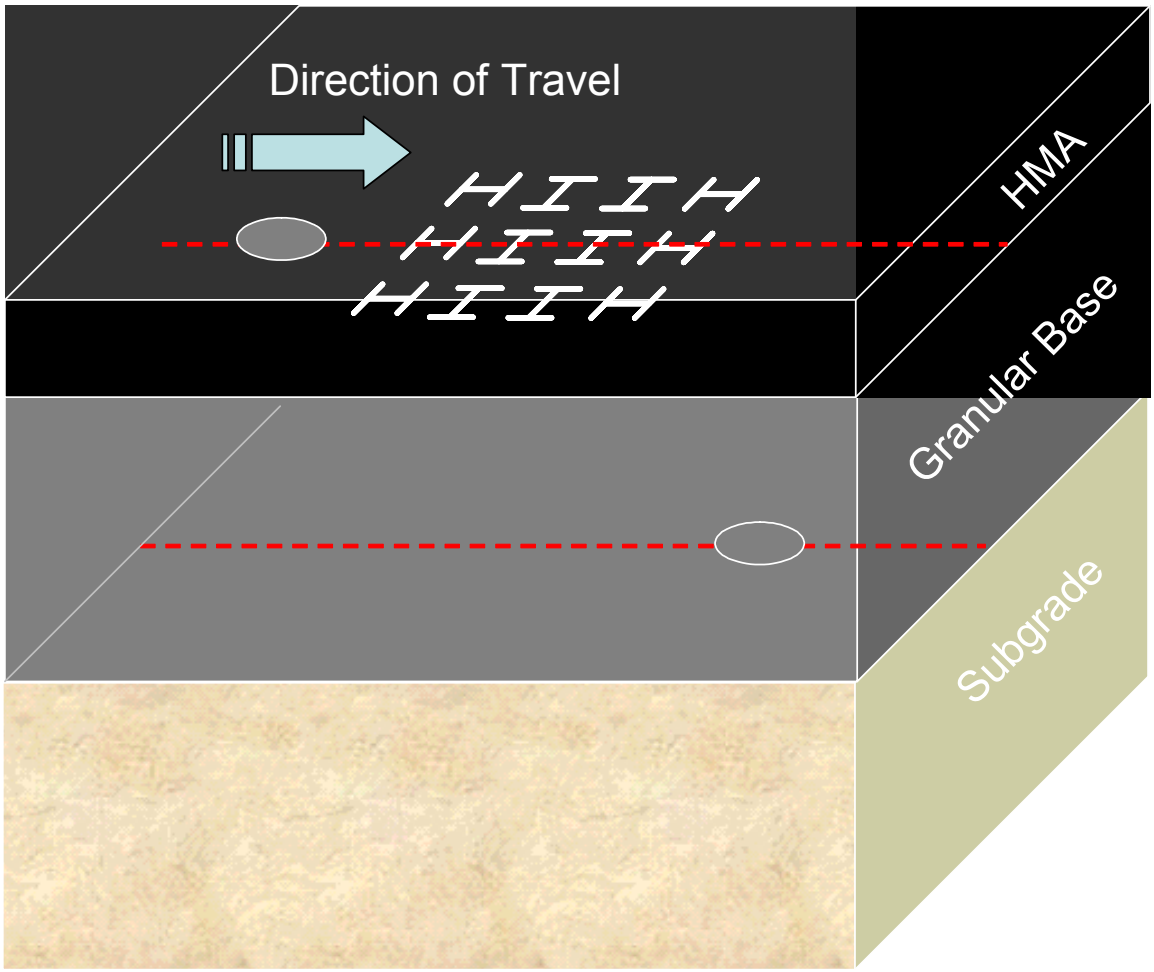

Figure 2.3 3D Generic Gauge Arrangement (Timm *et al.*, 2004).

The strain gauges were installed in two different layers in the locations marked in Figures 2.1 and 2.2. One set of gauges was at a depth of 7 inches, corresponding to the HMA and base interface. The second set of gauges was built into the pavement at a depth of 5 inches. In N8, this was the interface between the rich-bottom layer and the regular HMA structure.

Strain measurements were first taken on October 28, 2003, and continued to be taken once a week until either the pavement was too distressed to measure or the end of the experiment. Six different vehicles were used to load the pavement ranging from a triple trailer system to a simple box truck. Full descriptions of the trucks were documented by Priest (2005). Strains were measured locally for three passes of each vehicle, and then compiled and processed into a database. More information on this process was also documented by Priest (2005).

N7 AND N8 STRAIN COMPARISON

Since the only difference between N7 and N8 was the rich-bottom layer, and N8 failed while N7 did not, a comparison of the strains in the two sections seemed a logical starting

point for the investigation. First, comparisons were made between the strains at a depth of 7 inches (bottom of HMA) as shown in Figure 2.4. As can be easily seen, the strains in N7 are consistently greater than those of N8 at the bottom of the pavement section. The one exception is a brief spike from during December 2004 and January 2005. These data are consistent with previous findings about rich-bottoms yielding lower strains at the bottom of the pavement section due to increased density, thus prolonging the life of the structure.

The strain data from N7 followed the expected seasonal variability. Higher strains were recorded in the warmer months due to the pavement being softer. The colder months provided lower strain readings. However, this was not the case for N8. The strains at the base of N8 seem to be relatively unaffected by changes in season. The highest strain reading was recorded in January 2005, a time when the strains should have been low in comparison to warmer months. This indicates that there could be a problem with the strain measurements in the bottom of the HMA in section N8.

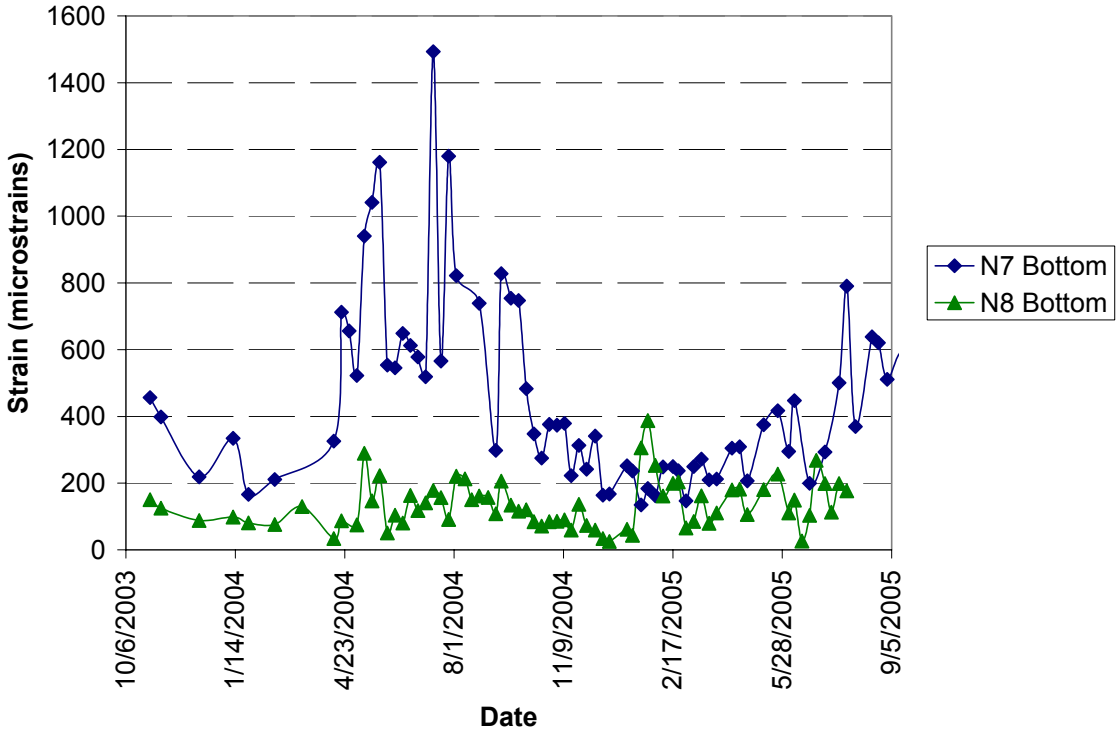

Figure 2.4 Strain Comparison for N7 and N8 at a 7 inch Depth for Truck 1.

As can be seen in Figure 2.5, the same results were not found for the strain measurements at a depth of 5 inches. For the remainder of this report, the term "lift strains" will refer to strain measurements made on top of the bottom lift. At the beginning of the study, the 5 inch depth strains tracked like those at a 7 inch depth. The N8 strains were lower than those of N7; however, on June 22, 2004, the strain values at the 5 inch depth in N8 surpassed those in N7 for the first time. Briefly, N8 strains fell below those of N7, but in October of 2004, the strain values spiked, and only one measurement beyond that date in N8 ever fell below those of N7.

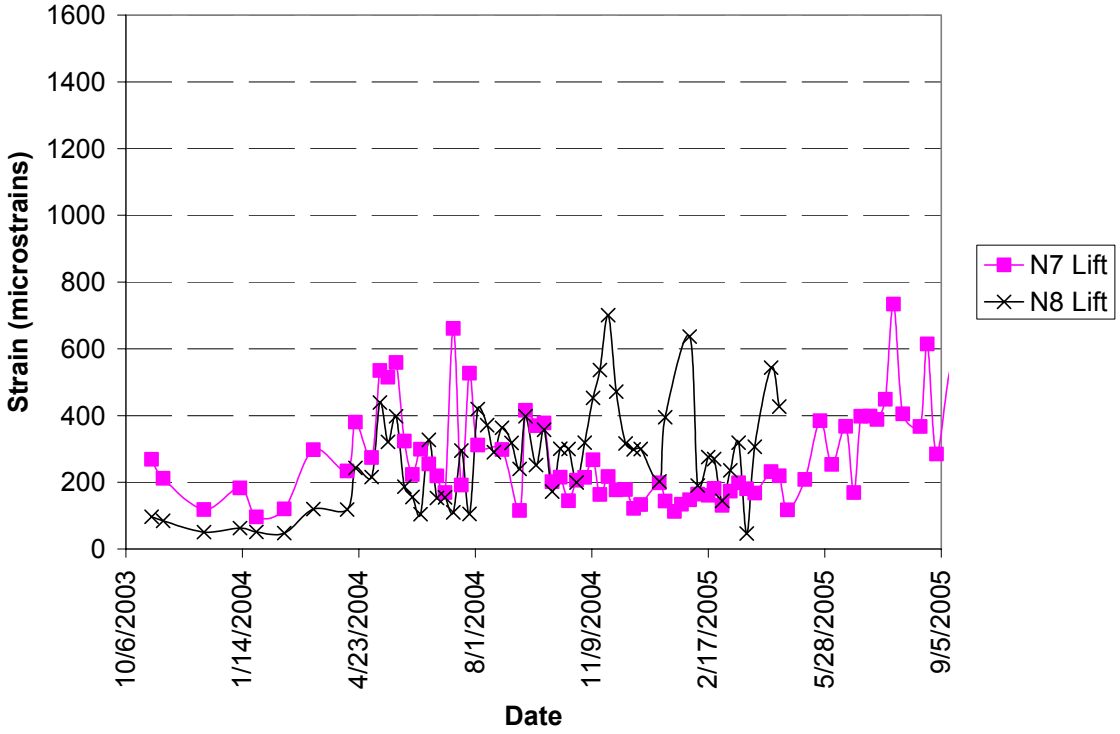

Figure 2.5 Strain Comparison for N7 and N8 at a Depth of 5 Inches for Truck 1.

INSIDE AND OUTSIDE WHEELPATH STRAIN COMPARISONS

Though N8 experienced more fatigue cracking than N7, it was not uniform throughout the test section. Specifically, the fatigue cracking in N8 was localized along the outside wheelpath; therefore, a comparison of wheelpath strains was launched to determine if the strain data supported this observation.

The strains at the bottom of section N8, as seen in Figure 2.6, typically showed a higher strain value along the inside wheelpath until around January 2005 where the strains in N8 jump from 43 to 306 microstrains in one week.

Figure 2.7 shows the strain data for the wheelpaths at the 5 inch depth. The outside wheelpath experienced slightly more strain from the inception of the project; however, in April 2004, the strain along the outside wheelpath spiked dramatically. It briefly experienced strains close to those along the inside wheelpath, but in August 2004, the outside wheelpath's strains once again increased dramatically. After this point, they never again recovered to those found along the inside wheelpath. Again, little seasonal variability was seen at both the bottom and the lift of N8. Figure 2.7 also shows that the outside lift strains became very erratic after November 2004. Recall that cracking first appeared in Section N8 in August 2004 which could have contributed to erratic strain readings.

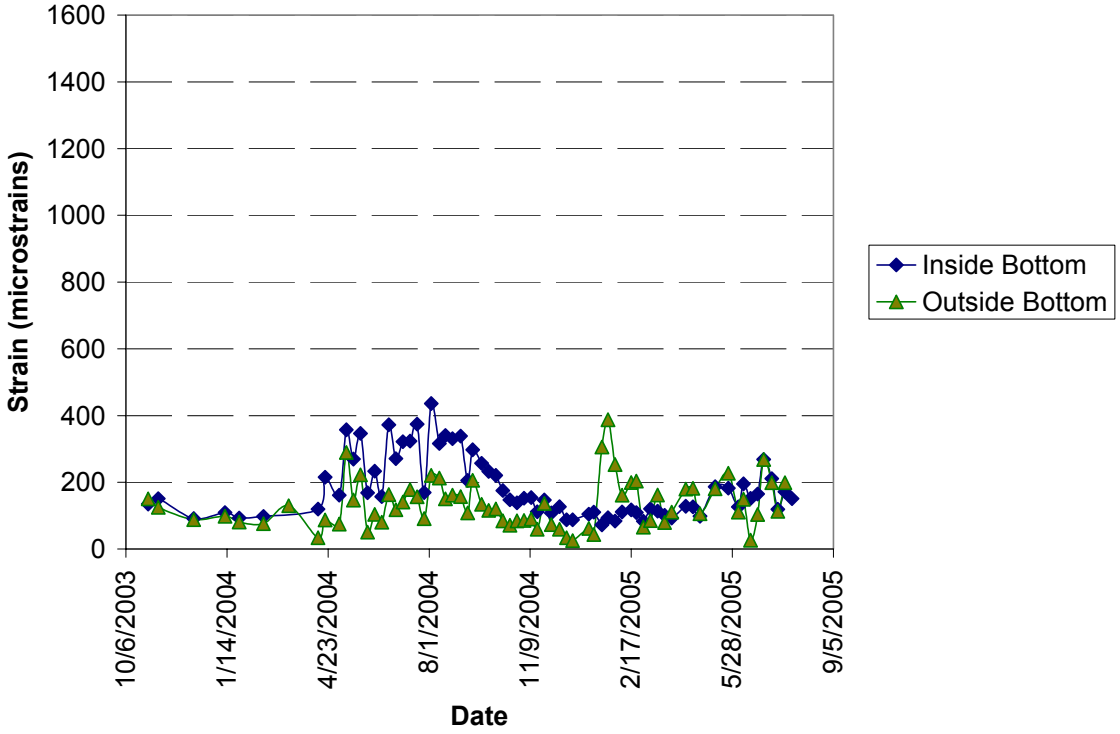

Figure 2.6 Strain Comparison of N8 Inside and Outside Wheelpaths at 7 Inches.

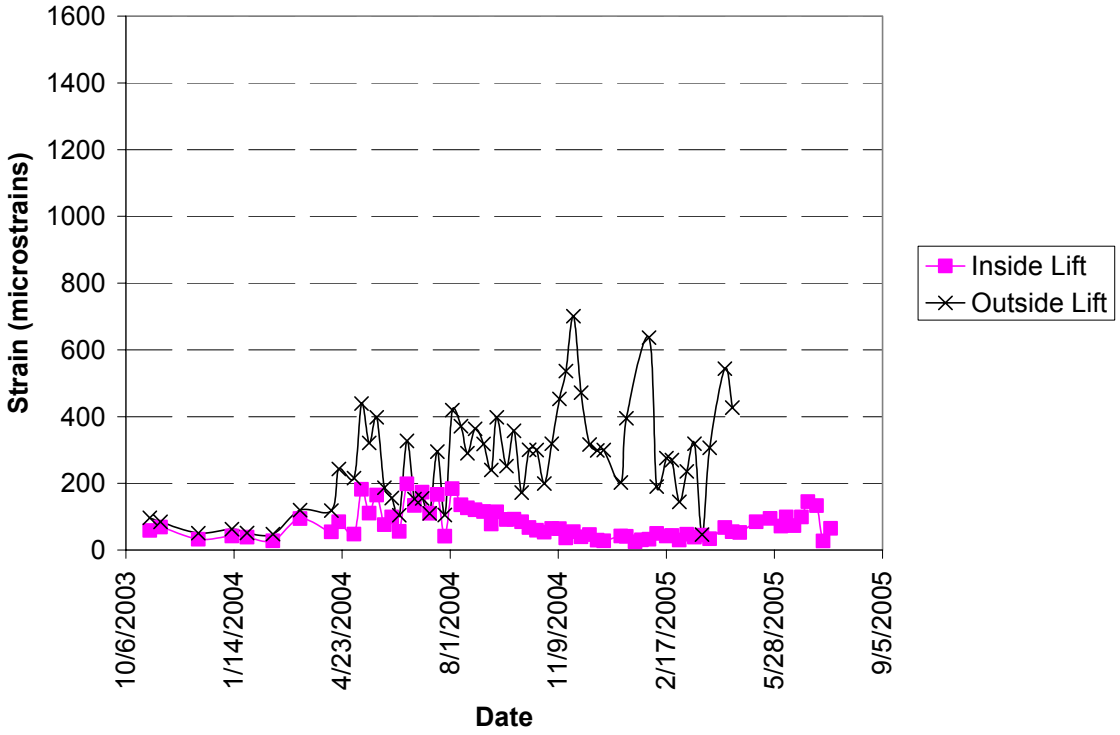

Figure 2.7 Strain Comparison of N8 Inside and Outside Wheelpaths of at 5 Inches.

5 INCH DEPTH AND 7 INCH DEPTH STRAIN COMPARISONS

Since the fatigue cracking was localized to the outside wheelpath of N8, it was important to determine what exactly was happening in the pavement at this point. The best way to determine this was a comparison of strains inside the pavement. The graphical results are displayed in Figure 2.8. As expected, greater strains are initially observed at the 7 inch depth of the pavement than at the 5 inch depth, which can be explained by layered elastic theory (Huang, 1993). However, in April 2004, something occurs inside the pavement that causes the 5 inch depth to experience more strain than the bottom of the pavement. In fact, the strain at 5 inches is greater than the 7 inch strain by over 300% at times. This is in opposition to layered elastic theory's prediction for well-bonded layers.

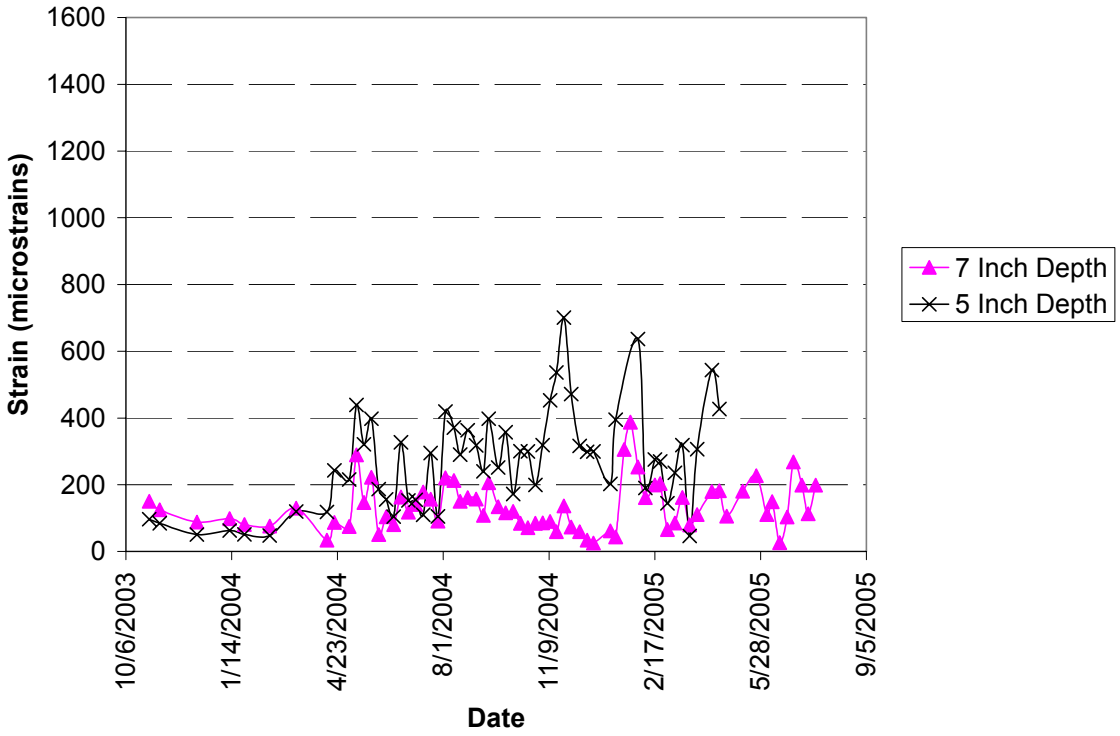

Figure 2.8 Strain Comparisons for Outside Wheelpath of N8.

WESLEA FOR WINDOWS ANALYSIS

Seeing this increase in strain and cracking caused speculation that debonding between the rich bottom and upper HMA layer may have been the cause of the deterioration. Prior to a physical forensic investigation, an analytical investigation was conducted with WESLEA for Windows.

WESLEA for Windows is a computer application using linear elastic theory to calculate pavement responses due to specific loads. The NCAT Test Track has fully documented material properties of each section from falling weight deflectometer testing that has been

conducted and then backcalculated to determine the structure's moduli (Timm and Priest, 2006). These average, temperature-corrected, moduli, along with surveyed depths, are found in Table 2.1. The lifts were given the same properties due to the nature of the backcalculation process. For the purposes of simulation, the structure was subjected to a 5,000 lb load and a tire pressure of 100 psi. The strains were calculated at depths of 5.3 and 7.3 inches for three different conditions.

The first condition involved a full bond between all layers of the pavement. Secondly, the SMA/HMA interface was allowed to debond while the HMA/Rich bottom layer did not have debonding. The third scenario involved a double slip where both layers debonded.

Figure 2.9 presents the theoretical strain profiles for a 7.3 inch pavement in all three of the scenarios listed. As shown in the figure, when full bond was specified during the analysis process, the pavement acted as one cohesive structure, but when slippage was specified, the pavement acted as two independent structures stacked on each other. Another effect of slippage was greater tensile strain values closer to the surface of the pavement.

Table 2.1 Structural Values for WESLEA Analysis

Layer	Modulus, psi*	Poisson	Height, in.	Bond Condition with Underlying Layer
SMA Lift	800680	0.35	1	Full Bond vs. Full Slip
HMA Upper Lifts	800680	0.35	4.3	Full Bond vs. Full Slip
Rich Bottom	800680	0.35	2	Full Bond
Base	10257.8	0.4	23	Full Bond
Subgrade	30000	0.45	Infinite	

*Note: Backcalculated moduli root mean squared error range from 0.58 to 6.0% with an average of 2.5%.

Next, in order to present the data in a useful form, a ratio of the strains, 7.3 inch (bottom) to 5.3 inch (lift), was calculated for both of the bond conditions. At full-bond, the strains produced a ratio of 2.078. If debonding were to occur at the SMA layer, the ratio of the two strains would be 2.48. The double slip incurs a ratio of 0.496.

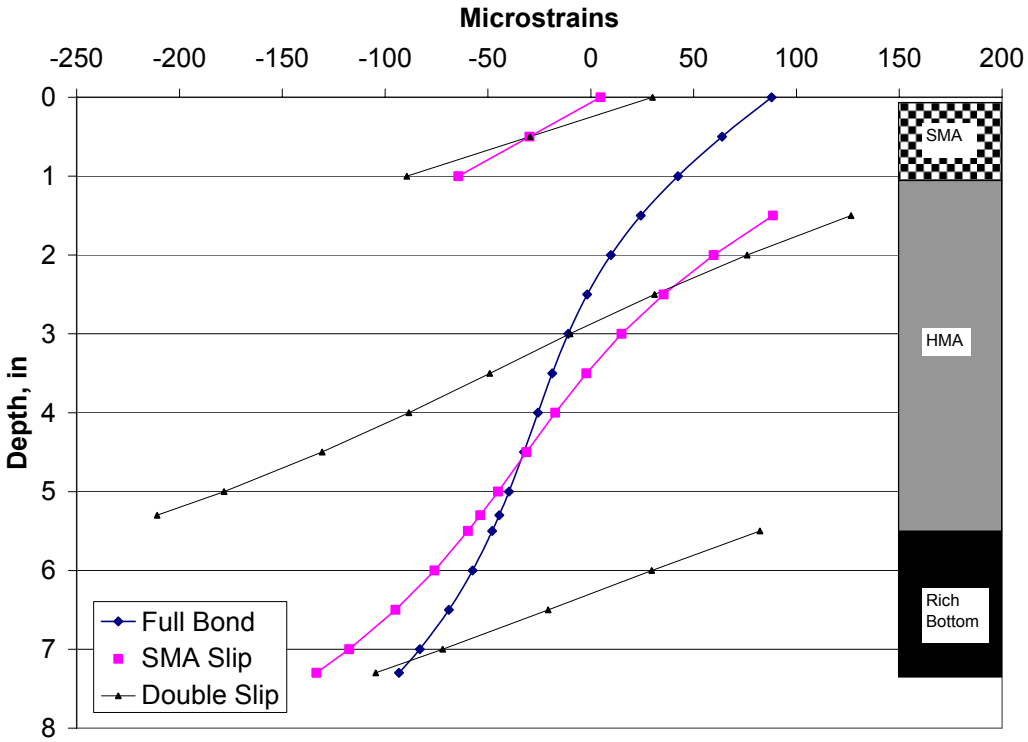

Figure 2.9 Theoretical Strain Profile of 7.3 inch Pavement.

ACTUAL VERSUS THEORETICAL

All of the measured strain values were averaged by truck for each day, and ratios were calculated as done for the WESLEA analysis. Ratios were calculated for both N7 and N8 in the outside wheelpath. The ratios were then plotted over time with the WESLEA averages superimposed in Figures 2.10 and 2.11. Inspection of these figures shows that the strain ratios for N7 compare favorably to WESLEA ratio for full-bond, as summarized in Figure 2.12. The measured average ratio for N7 was 1.84. The strain ratios for N8 graphically relate to the WESLEA double slippage ratios. The measured average strain ratio for N8 was 0.542 compared to the WESLEA value of 0.496. If the ratio for N8 is taken from the date when the 5 inch depth strain first surpassed that of the 7 inch strain, the average ratio is 0.49. This analysis supports the idea that debonding occurred in N8 while N7 remained fully bonded. Neither of the values is similar to the SMA slippage only ratio of 2.48.

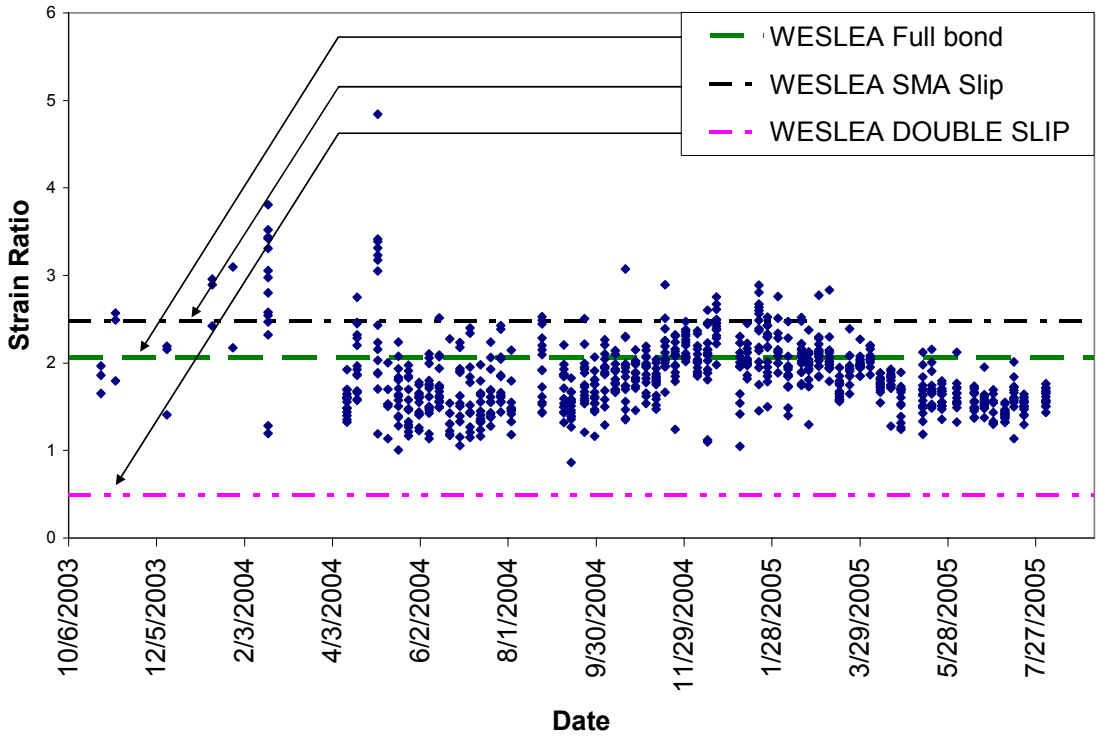

Figure 2.10 N7 Strain Ratios Versus Theoretical Ratios.

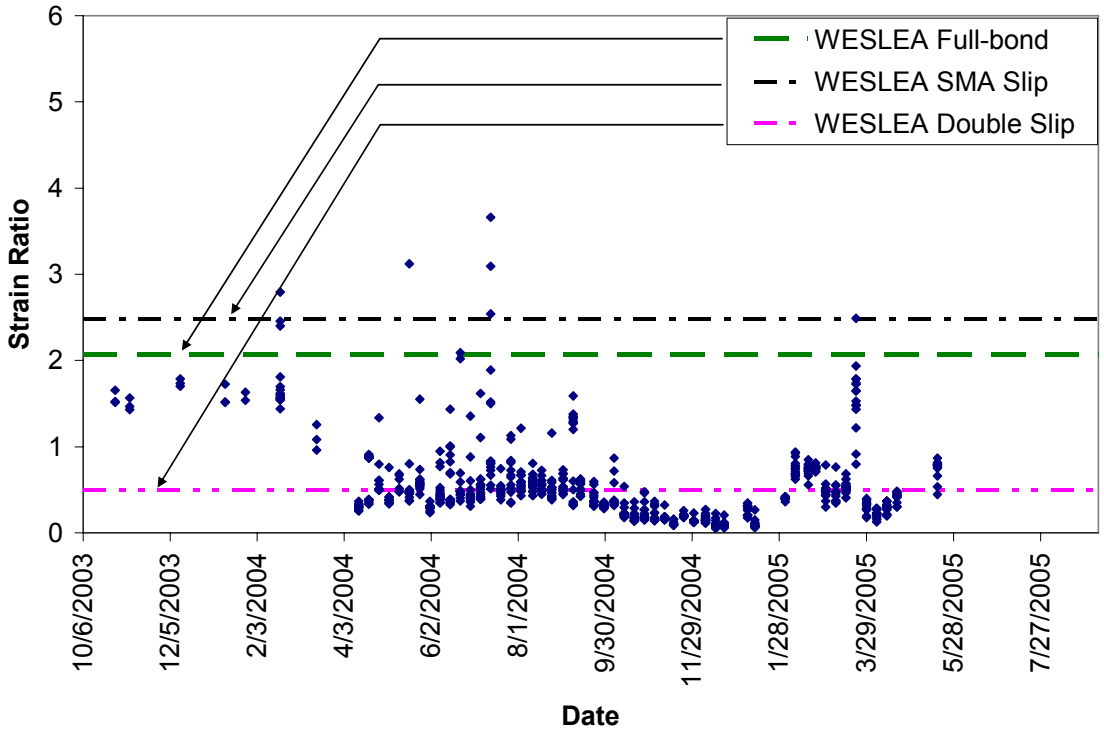

Figure 2.11 N8 Strain Ratios Versus Theoretical Ratios.

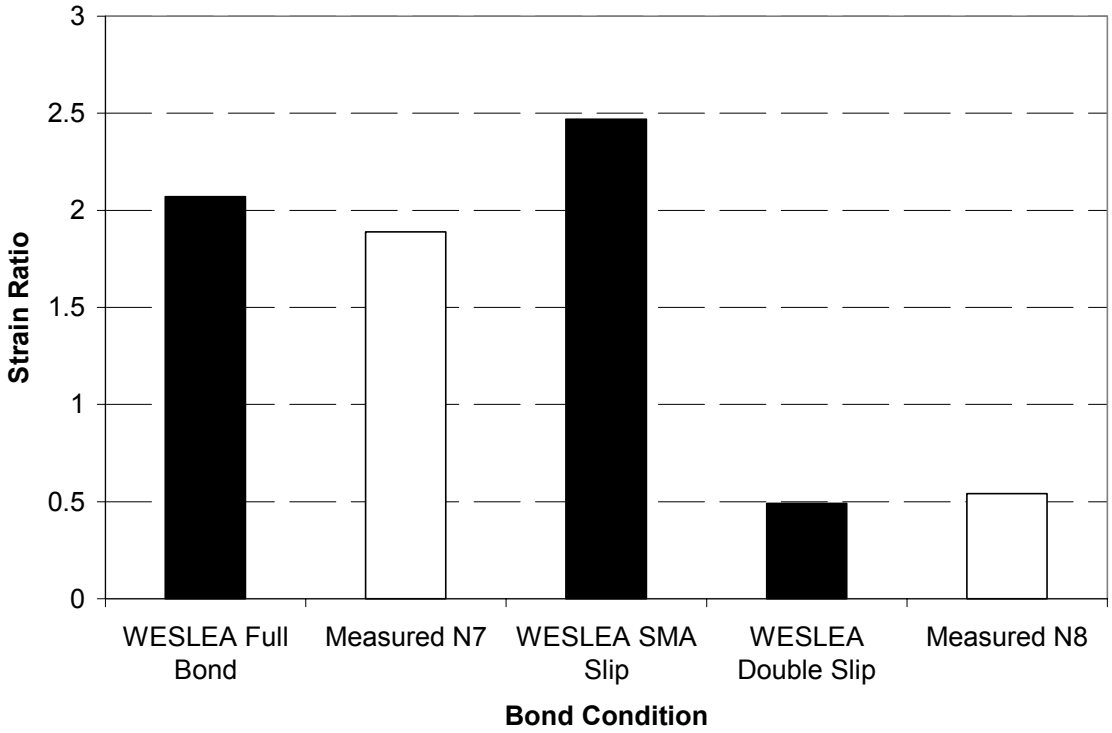

Figure 2.12 Strain Ratio Summary.

STRAIN STUDY SUMMARY

Graphical comparisons were made to try to determine the origin of the N8 deterioration. When dynamic strain values were compared to those from N7, the strain readings at the 7 inch depth were lower than those found in N7. But the strain values at the 5 inch depth in N8 surpassed those from N7 in June of 2004 after tracking similarly. Like the N7 comparison, when the strains in each wheelpath of N8 were compared, the 7 inch depth strains tracked near each other, but in April of 2004, the strain values 5 inches below the surface began to become erratic in the outside wheelpath. A final comparison was made between strain at depths of 7 inches and 5 inches in the outside wheelpath of N8. One would expect the strains to be greater at the bottom of the pavement; however, the strain values at 5 inches soon exceeded those of the bottom.

A theoretical simulation using the material properties of N8 was set up using WESLEA for Windows to determine theoretical strains at the lift and bottom of the pavement with conditions involving full bond between layers and full slip. Ratios of 7 inch strains to 5 inch strains were then calculated and compared to those recorded from the dynamic strain data. Though close agreement between measured and theoretical strains was observed and supported the double layer-slippage hypothesis, further forensic investigation, described in the following sections, was warranted to more fully investigate and explain the cracking in N8.

CHAPTER 3 - TRENCH STUDY

BACKGROUND

While theoretical and measured strain ratios suggested the occurrence of debonding in the pavement structure, physical proof of this debonding would further substantiate the hypothesis. Therefore, three locations with varying levels of fatigue distress were chosen to undergo trenching and crack mapping.

Trench 1 (Figure 3.1) was cut through the middle of the gauge array. This location had heavy fatigue cracking, and base material pumping from the cracks could be seen. Trench 2 (Figure 3.2) was cut just upstream of the instrumented area. This location had experienced fatigue cracking, but not to the extent of Trench 1. Trench 3 (Figure 3.2) was located just inside N8 where no evidence of cracking was seen.

Figure 3.1 Location of Trench 1.

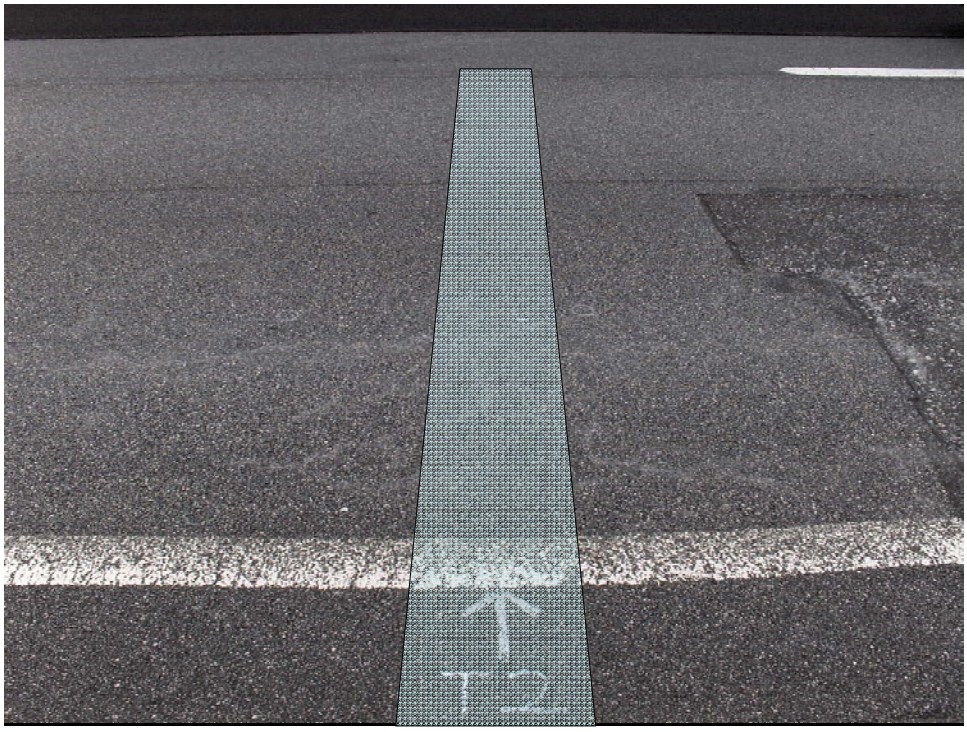

Figure 3.2 Location of Trench 2.

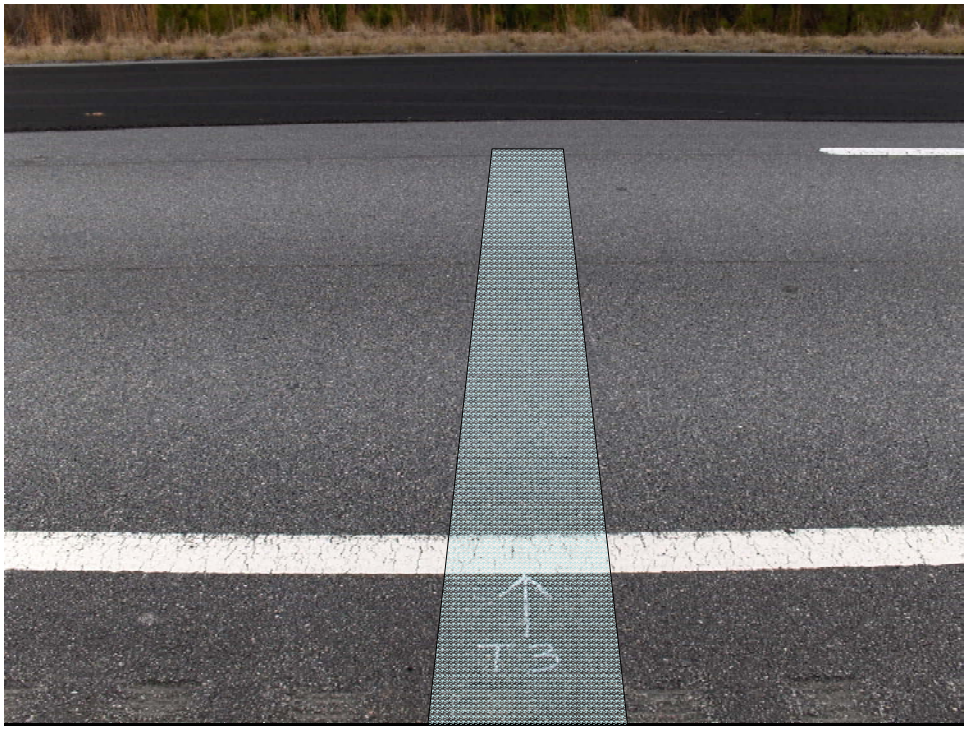

Figure 3.3 Location of Trench 3.

On March 14, 2006, the three trenches were cut and ran transversely across the pavement from the outside edge to the centerline in locations shown in Figure 3.4. The trenches were cut, as seen in Figure 3.5, to a depth just below the HMA layer to enable inspection

of the bottom of the rich-bottom layer. Once the trenches were cut, a backhoe was used to remove the asphalt in slabs (Figure 3.6). Upon removal of the slabs in Trench 1, the presence of debonding was physically confirmed at the SMA/HMA interface, Figure 3.7.

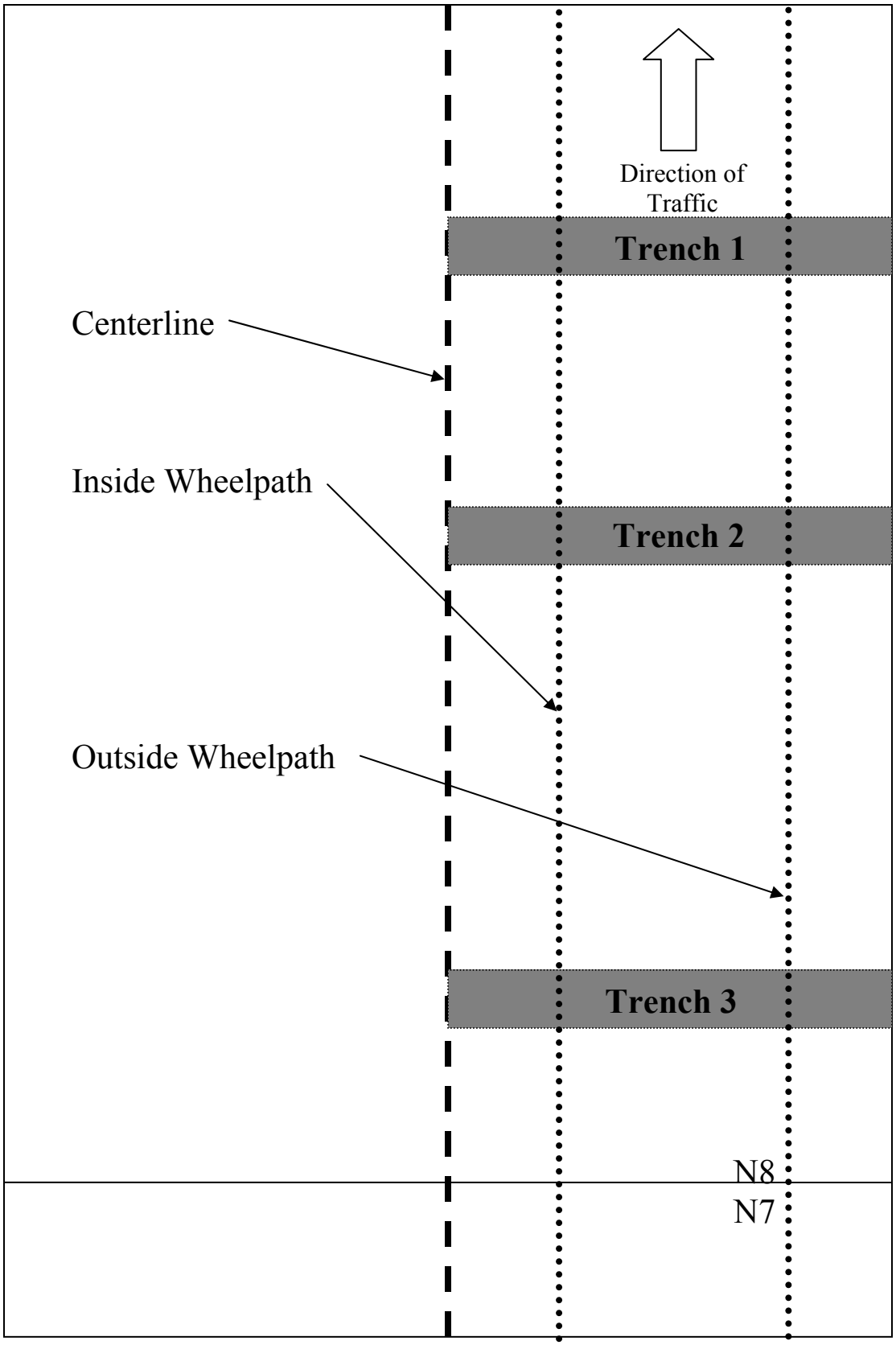

Figure 3.4 Trench Locations.

Figure 3.5 Cutting Trench 1.

Figure 3.6 Excavating Trench 1.

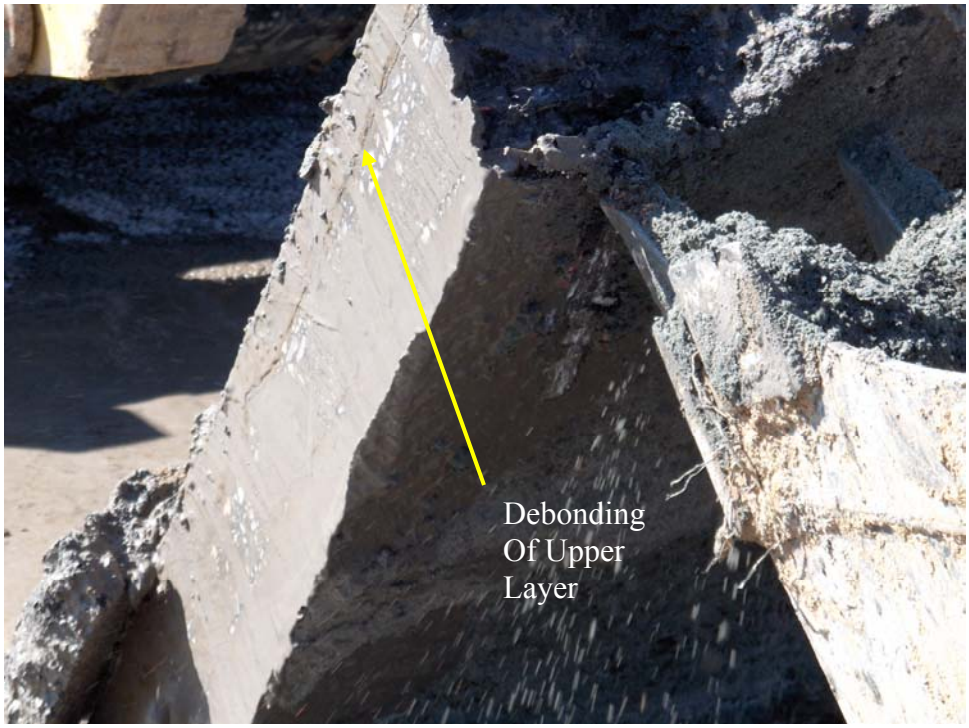

Figure 3.7 Physical Debonding of Slab from Trench 1.

A more thorough investigation was needed to further substantiate the theory of layer debonding. It was feared that despite the care taken in slab removal, the asphalt could have been damaged. Debonding can be seen in Figure 3.7 along the top of slab. To compensate for this, on March 22, 2006, a careful crack mapping investigation along the inside walls of the trenches was performed. Each trench was drained and cleaned to make the cracks visible for inspection. Every crack visually discernable was then marked and documented for all three trenches. The next three sections provide the results of these investigations.

TRENCH ONE

Trench 1 is shown in Figure 3.8. Trench 1 was the location where the heaviest fatigue cracking existed, specifically along the outside wheelpath. The lower layers of the pavement structure showed the heaviest fatigue damage, as well.

The outside wheelpath showed signs of heavy fatigue cracking; however, the cracking was mainly contained to the upper five inches of the pavement (Figure 3.9). The top inch of SMA crumbled along the edge of the cut due to the severity of the fatigue damage. Few cracks propagated into the rich-bottom layer. The outside wheelpath showed signs of debonding between the SMA layer and the rest of the pavement. It is also interesting to note the bifurcated crack shown in Figure 3.8c. It appears that the crack may have initiated above the rich-bottom layer and propagated downward. This would support the idea of a slippage problem at the bottom of the pavement.

a)

b) **c)**

Figure 3.8 Trench 1 West Face.

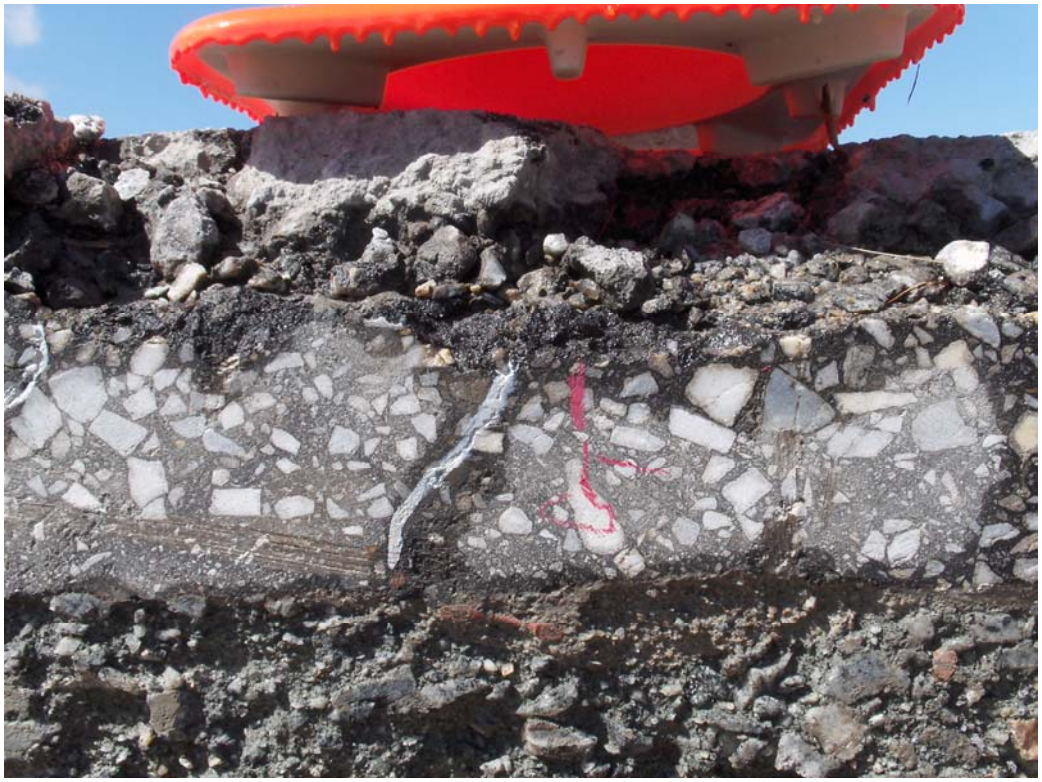

Figure 3.9 Fatigue Deterioration of Trench 1.

TRENCH TWO

Trench 2 (Figure 3.10) was cut in a location where only some fatigue cracking and pumping was seen at the pavement surface. The crack mapping of Trench 2 again showed some evidence of fatigue cracking in the upper layers of the pavement. Cracks were confined from the top of the pavement to the rich-bottom interface. The rich-bottom layer had not been damaged due to the loading.

Figure 3.10b illustrates a crack that could have been the result of two possible scenarios. The crack could have initiated on top of the rich-bottom, propagated up to the SMA/HMA interface and then followed this potentially weak interface, or the crack could have begun at the weaker layer and propagated from there. While debonding was present, the cracks between the previously bound layers were not as wide as those found in the first trench.

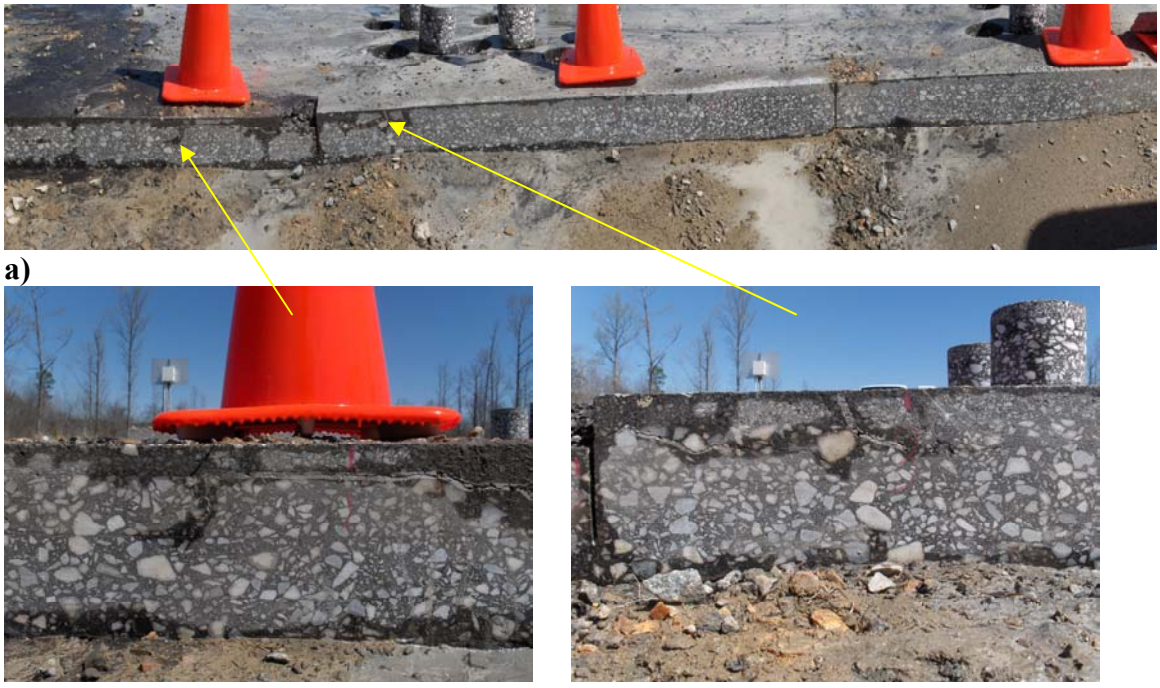

a)

b) **c)**

Figure 3.10 Trench 2 East Face.

TRENCH THREE

Trench three, shown in Figure 3.11, was cut in a location just inside N8 where virtually no surface damage had been observed. The crack mapping investigation provided evidence that the interior of the pavement had not been damaged either. The SMA, HMA, and rich bottom layers were still bonded and free of fatigue cracking.

Figure 3.11 Trench 3 West Face.

SUMMARY OF TRENCH INVESTIGATION

Three trenches were cut in N8 at locations of varying surface distress due to either fatigue cracking or pumping. The trenches provided supportive physical data that debonding had occurred in the areas of the section that contained moderate to severe fatigue cracking. In every case where interior damage had occurred, fewer cracks were found in the rich-bottom layer than in the upper stratums of the pavement. This supports the belief that the rich-bottom layer served its purpose by being more fatigue-resistant to the imposed strain levels.

CHAPTER 4 - BOND STRENGTH ANALYSIS

CORING

On Tuesday, March 21, 2006, the third analysis procedure for the N8 forensic investigation began. This analysis was an investigation of bond strengths at different locations throughout N8 and N7 to see if bond strengths varied with the degree of fatigue cracking.

In order to pursue this analysis procedure, forty 6 inch diameter cores were taken that could be tested for bond strength. Ten cores were taken near each trench, and ten control cores were taken from N7 as shown in Figure 4.1. Five cores came from each wheelpath with the exception of Trench 1. The extent of the fatigue damage at Trench 1 made it physically impossible to remove a core intact; therefore, five cores were taken downstream (relative to the direction of traffic) and five were taken upstream of the trench location in the inside wheelpath. The core groupings for trench 1 were labeled "A" and "B" corresponding to after and before the trench, respectively.

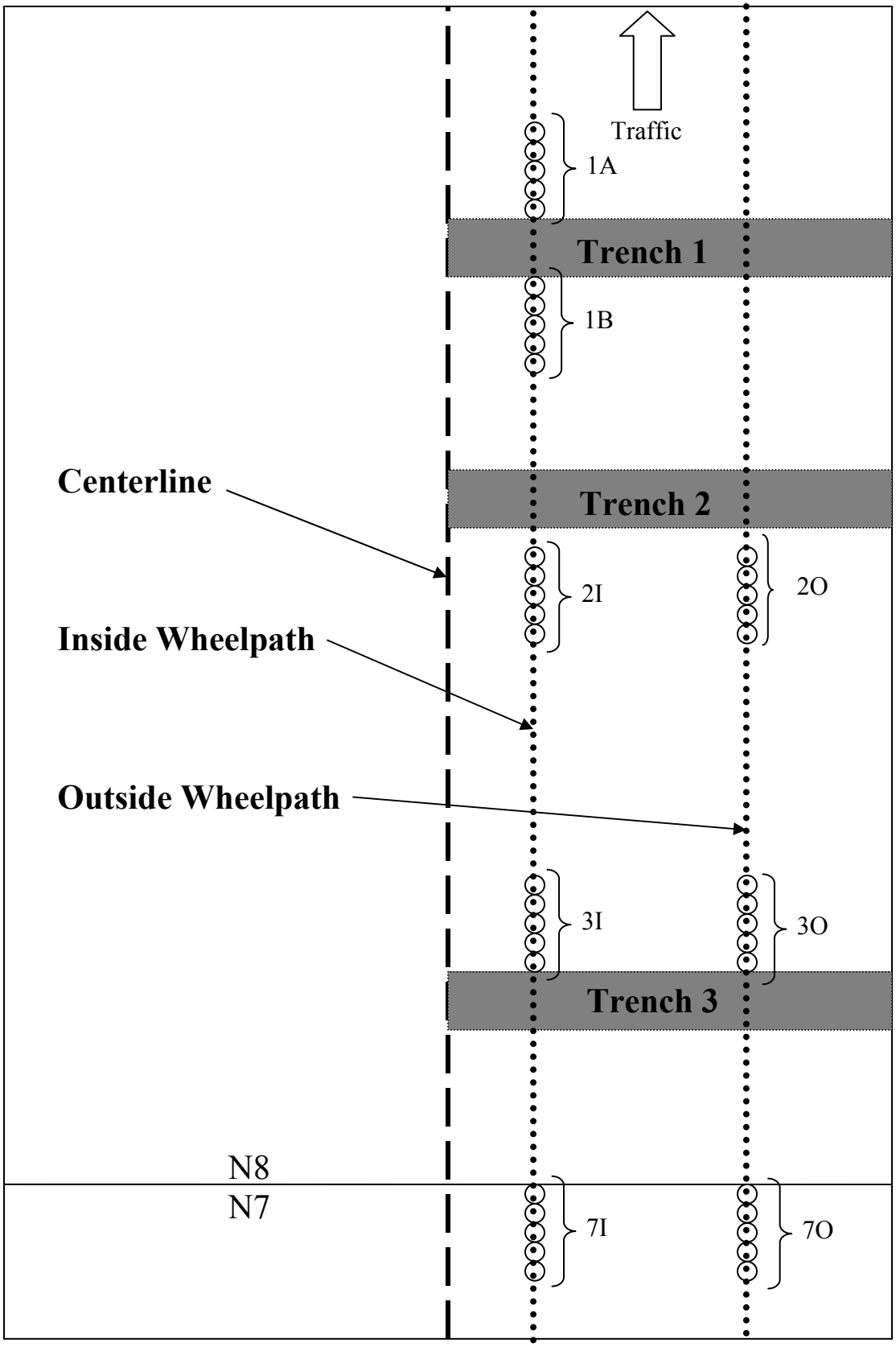

Figure 4.1 Core and Trench Locations.

The cores were labeled by trench, wheelpath location, and longitudinal location from 1 to 5. Those labeled 1 were furthest downstream of the trench location as can be seen in Figures 4.2 and 4.3. Upon completion of the coring process, the cores were transported back to the NCAT laboratory for bond strength testing using a simple shear apparatus in a Marshall load frame.

Figure 4.2 Cores Taken Before Trench 1.

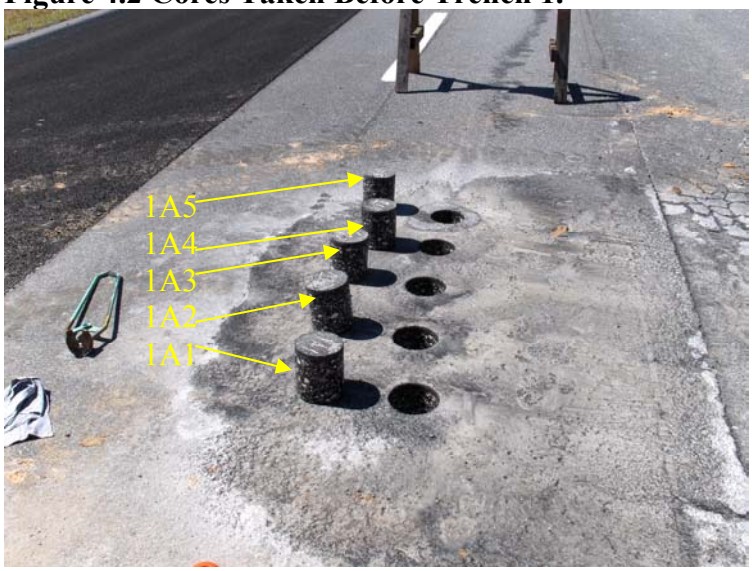

Figure 4.3 Cores Taken After Trench 1.

BOND STRENGTH TESTING

Bond strength testing was conducted at the NCAT laboratory. In order to test for bond strength, the 6 inch cores were loaded into a fitted collar (Figure 4.4). This collar applied a shear force to a desired portion of the core while holding the rest of the core fixed (Figure 4.5). A Marshall Pine Recording Test Press, shown in Figure 4.6, was used to apply the shear force on the sample as specified by ALDOT's draft test method entitled the *Standard Test Method for Determining the Bond Strength Between Layers of an*

Asphalt Pavement. More information on this type of testing is documented by West *et al*. (2005).

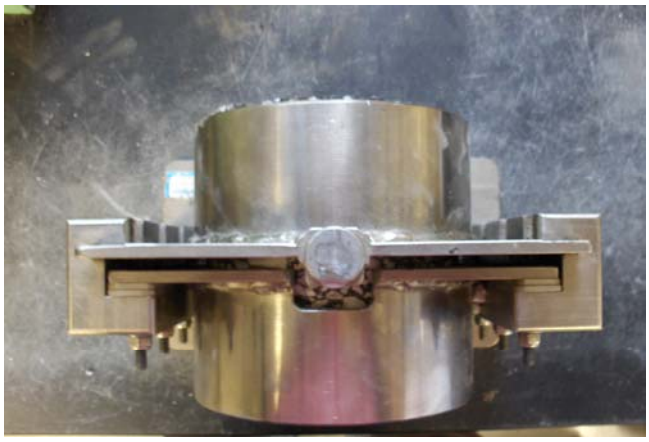

a) View from Above

b) View from Side

Figure 4.4 Core Fitted in Shear Collar.

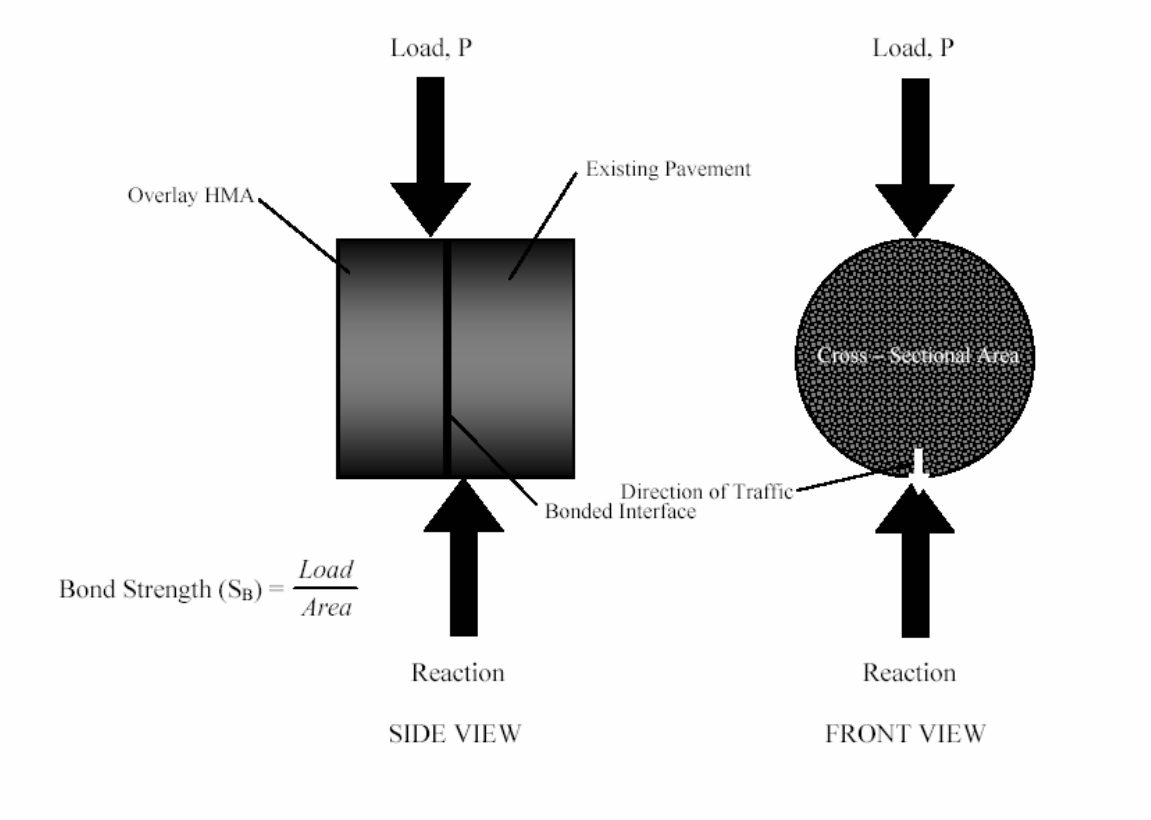

Figure 4.5 Loading Scheme Used for Bond Strength Test (West *et al.*, 2005).

Figure 4.6 Marshall Pine Press.

Two locations were chosen to test the bond shear strength of the core. The first location was one inch below the surface at the SMA/HMA interface. This location showed the most debonding during the trenching analysis; therefore, it was important to quantify the bond strength at this depth. The second location was at a depth of 5 inches corresponding to the HMA/rich-bottom interface. These locations are seen in Figure 4.7.

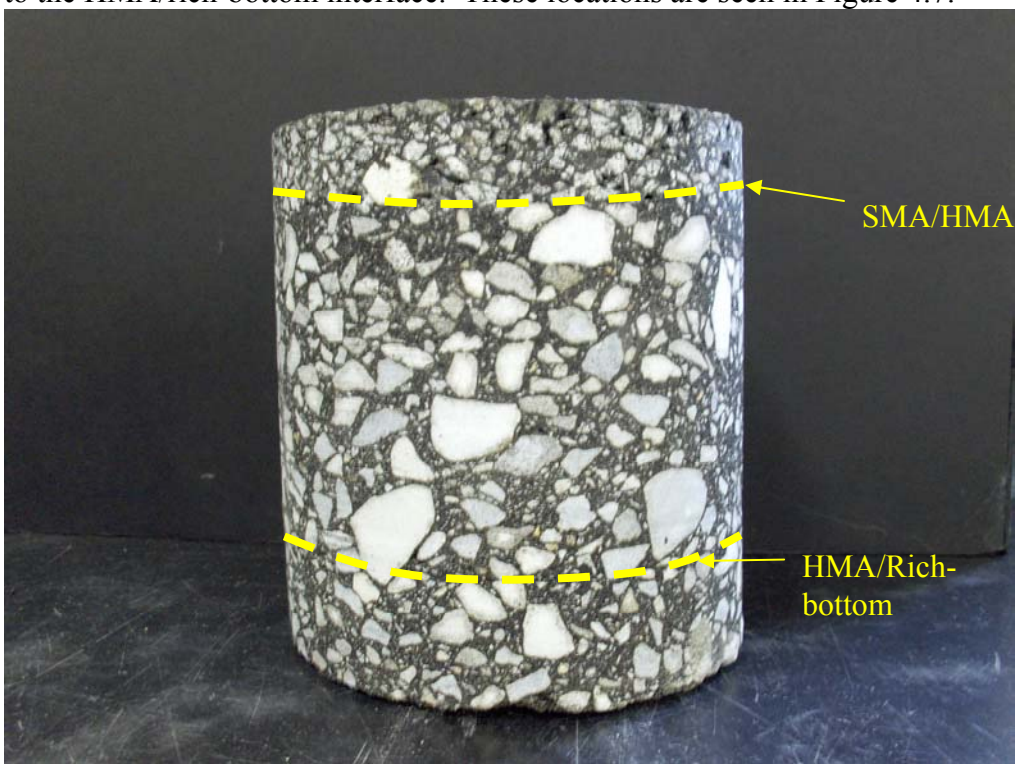

Figure 4.7 Bond Strength Test Locations.

The Marshall Pine Recording Test Press has varying maximum load capacities depending on the type of test being run. For bond strength, the highest maximum load value (10,000 lb) was chosen. Each core was subjected to a constant strain rate of 2 inches per minute, and the loads were recorded. Using this method, the maximum shear load for the sample was determined. All of the raw graphs for the tests can be found in Appendix A. The maximum shear capacity was then divided by the area of shear plane to determine the shear strength in psi as illustrated in this example:

Core 1A1 SMA/HMA Ultimate Shear Load (USL):	4000 lbs
Core 1A1 SMA/HMA Diameter:	6 inches
Area of Core 1A1: $A = \pi * r^2$	28.27 in^2
Core 1A1 Shear Strength for SMA/HMA: $S = \frac{USL}{A}$	141.47 psi

WESLEA SHEAR STRESS

A brief analysis was conducted of a 7 inch pavement using the material properties given in the previous WESLEA analyses to determine the amounts and locations of shear forces on the pavement structure. Shear values were calculated at every ½ inch depth aligned

along the outside wall of the tire. This analysis (Figure 4.8) showed that the highest levels of shear would be concentrated just below the SMA layer of the pavement while lower shear stresses occurred at the HMA/Rich-bottom interface. This means that the bond strength between the SMA and HMA is critical. It is also important to note that the simulation lacking full bond resulted in the rich-bottom acting independently of the upper HMA layers.

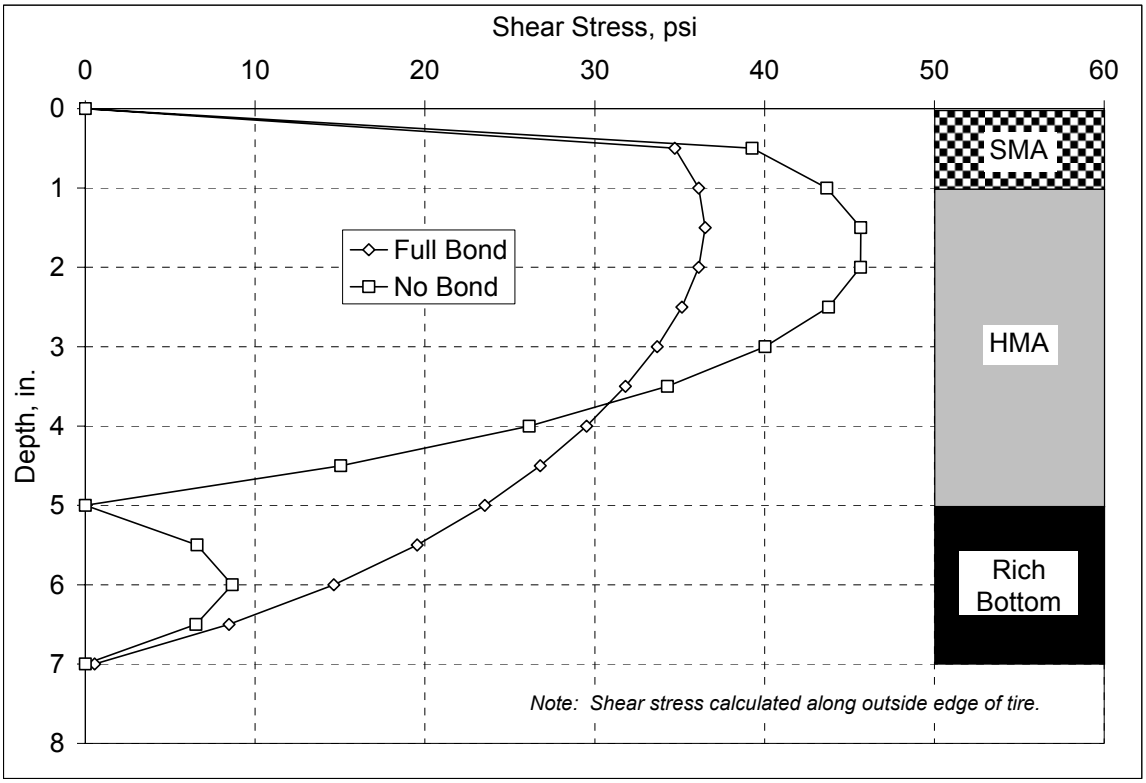

Figure 4.8 WESLEA Shear Study Results.

BOND STRENGTH TEST RESULTS

Bond strength tests were run on all 40 cores at the 1 inch depth and 5 inch depths. The strength results are found in Appendix B while their summary statistics are found in Table 4.1 and Figure 4.9. Figure 4.1 can again be referred to for core locations.

Table 4.1 Statistics of Bond Strength Testing

Section	Trench	Location	Depth	Average Strength, psi	Standard Deviation, psi
N8	1	A	1"	157.10	47.54
			5"	301.19	21.35
		B	1"	148.97	43.79
			5"	266.18	20.52
	2	I	1"	126.48	17.16
			5"	286.34	5.71
		O	1"	101.15	45.54
			5"	243.12	18.26
	3	I	1"	261.86	66.82
			5"	299.42	11.37
		O	1"	165.31	29.21
			5"	277.42	43.52
N7	7	I	1"	152.79	4.02
			5"	279.76	9.97
		O	1"	128.81	20.77
			5"	280.96	20.45

(Note: A = After Trench, B = Before Trench, I = Inside Wheelpath, O = Outside Wheelpath)

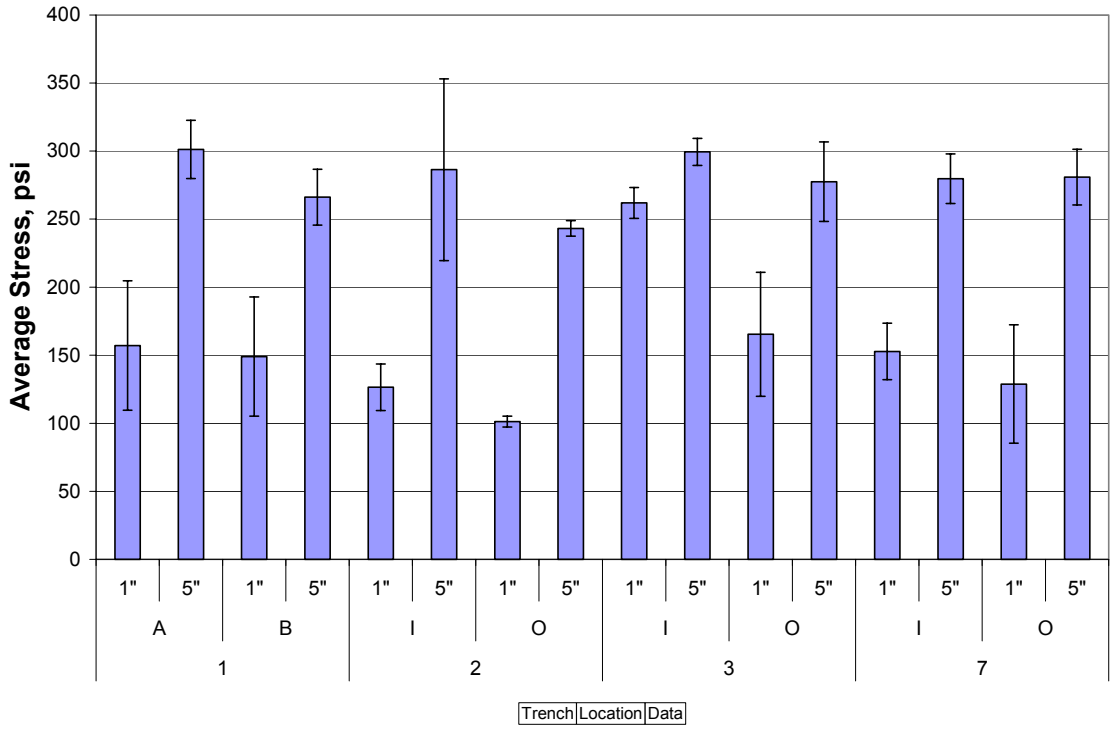

Figure 4.9 Graphical Statistics of Bond Strength Tests.
(Note: A = After trench, B= Before Trench, I = Inside Wheelpath, O = Outside Wheelpath)

One can observe from Table 4.1 that the average bond strengths at the rich-bottom interface were always higher than those at the SMA interface. In many cases, 5 inch depth strengths were nearly twice that of the 1 inch depth. However, this may be due to the nature of the test. ALDOT's specifications for this test require a 2 inch depth, but the SMA/HMA interface was only at a depth of 1 inch. It also appears that the inside wheelpath's average strengths were greater than those along the outside wheelpath. The inside wheelpath's bond strength averages were 180 psi for the 1" depth and 289 psi for the five inch depths while the outside wheelpath's strengths were 132 psi and 276 psi. Both of these conclusions are supported by the trenching and WESLEA analyses. More physical damage was seen along the outside wheelpath and near the top of the pavement structure. In relation to WESLEA, when debonding occurred, the strains in the upper layers of the pavement increased; however, when the measured bond strengths are compared to the theoretical shear stresses imposed on the pavement (Figure 4.8, Table 4.1), the actual bond strengths are all at least twice as great as the theoretical maximum shear stress seen in the pavement.

WHEELPATH STATISTICAL COMPARISONS

Statistical t-tests were conducted at a 95% confidence level to determine if statistical differences between the average bond strengths at the cored locations could be found. If the bond strengths were found to be statistically different, this might partially explain why some locations deteriorated while others did not.

The first comparison, summarized in Table 4.2, was made by comparing the bond strength's of the wheelpaths in each section. In a wheelpath comparison, statistically significant differences were seen at the 5 inch depth of Trench 2, where some damage had been seen, and at the 1 inch depth of Trenches 3 and 7 where no damage was visually found. One would have expected more significant differences to be found where more damage had occurred. Fatigue cracking and pumping were seen at the top of Trench 2 along the outside wheelpath, but that location recorded a high p-value.

Table 4.2 t-test Results for Wheelpaths

Core Set 1	Average, psi	Core Set 2	Average, psi	p-value	Significant
2OT	165	2IT	126	0.278	No
2OB	243	2IB	286	0.001	Yes
3OT	165	3IT	262	0.018	Yes
3OB	277	3IB	299	0.306	No
7OT	129	7IT	153	0.035	Yes
7OB	281	7IB	280	0.909	No

(Note: O = Outside Wheelpath, I = Inside Wheelpath, T = 1" Depth, B = 5" Depth)

TRENCH LOCATION COMPARISONS

The next comparison compared bond strengths of trench locations within N8. Table 4.3 contains the results of the 95% confidence level statistical t-tests. The trench location study within showed that the most significant differences in bond strength were found at

the 1" SMA/HMA interface. Both wheelpaths showed significant differences while neither of the wheelpaths showed significant differences at the 5 inch depth.

Table 4.3 t-test Results for Trenches

Core Set 1	Average, psi	Core Set 2	Average, psi	p-value	Significant
2IT	126	3IT	262	0.002	Yes
2OT	165	3OT	165	0.029	Yes
2IB	286	3IB	299	0.051	No
2OB	243	3OB	277	0.143	No

(Note: O = Outside Wheelpath, I = Inside Wheelpath, T = 1" Depth, B = 5" Depth)

N7 TO N8 COMPARISON

The third statistical comparison was conducted by comparing the trenches in N7 to those in N8. These values are found in Table 4.4. No real conclusions can be summoned from this table. Two comparisons from both trenches proved to be statistically different; however, more differences in bond strength were seen at the SMA/HMA interface than at the rich bottom/HMA interface.

Table 4.4 t-test Results for Section Comparison

Core Set 1	Average, psi	Core Set 2	Average, psi	p-value	Significant
2IT	126	7IT	153	0.001	Yes
3IT	286	7IT	153	0.007	Yes
2OT	165	7OT	129	0.252	No
3OT	165	7OT	129	0.052	No
2IB	286	7IB	280	0.236	No
3IB	299	7IB	280	0.020	Yes
2OB	243	7OB	281	0.015	Yes
3OB	277	7OB	281	0.873	No

(Note: O = Outside Wheelpath, I = Inside Wheelpath, T = 1" Depth, B = 5" Depth)

TOP TO BOTTOM COMPARISON

A final statistical comparison was made comparing the strengths at the 1 inch depth to those at the 5 inch depth. This was conducted using a paired t-test at a 95% confidence level. This test was to confirm the visual differences that were noted in the physical strengths from Figure 4.9. The test did conclusively confirm that statistical differences were notable between the bond strength at the top and bottom of the core specimens. The p-value returned was $2.04E^{-17}$.

PHYSICAL FAILURE COMMENTS

The Marshall Pine Recording Test Press is set up to hold one portion of an asphalt core in-place while subjected another portion of it to an ever increasing shear load. One

would expect, under loading such as this, for a smooth shear plane to be the result of a failed specimen; however, this was not always the case.

The cores from Trench 1 failed as expected. Figures 4.10 and 4.11 show the clean break exposing the rich black asphalt when the cores from Trench 1 were sheared. Cores from Trench 2 failed differently as shown in Figures 4.12 and 4.13. When shearing the 1" SMA layer from the core, many of the cores sheared at another location between 0.5 to 1 inch below the SMA interface. At a depth of 1 inch, the exposed surface was a rich black color. However, at the second break, the core was feeble and gray (Figure 4.14). Upon further inspection of the core, small cracks were seen in its base. The gray color could be the presence of fines that were ground from the pavement structure due to the debonding of the upper layers. Another effect of the shear loading was crack propagation throughout the top layer of SMA that was being sheared off (Figure 4.15).

Figures 4.10 Core 1A1.

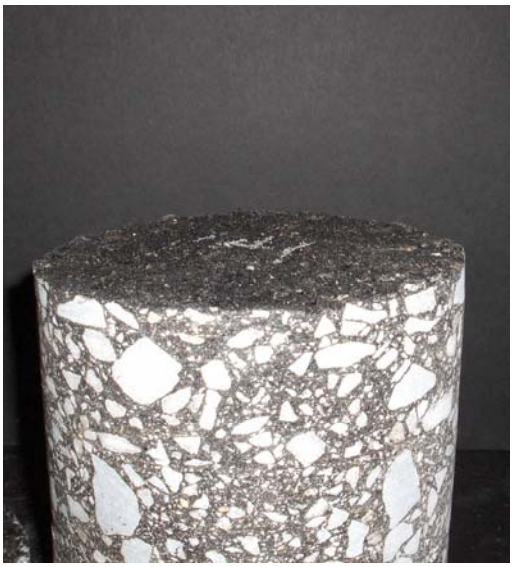

Figure 4.11 Clean Break of Core 1A1.

Figure 4.12 Core 2O1.

Figure 4.13 Extra Break in Core 2O1.

Figure 4.14 Gray Layer of Second Break.

Figure 4.15 SMA Damage from Trench 2.

Trench 3 provided clean breaks along the lifts as expected. The failure mode for the N7 cores was once again different from the previous three. While the other samples failed

along lift interfaces at both depths, the failure at the 5inches depth of N7 was different. The top sheared off along the SMA interface, but instead of having a clean break along the lift at 5 inches, the failure line occurred more along the edges of the aggregates. In many cases, the bottom portion of N7's samples did not even shear off completely, but rather just shifted out of position slightly. This is shown in Figure 4.16.

Figure 4.16 Core from N7.

GRAPHICAL RESULTS

The physical failure results can be explained somewhat by examination of the graphs produced by the Marshall Pine Recording Test Press. The machine was not immediately stopped upon a specimen's reaching its maximum load. The cores that came from N8 had one consistent theme to their loading graphs. Upon reaching the maximum shear load, the cores could no longer support the constant strain, and the load values immediately decreased (Figure 4.17).

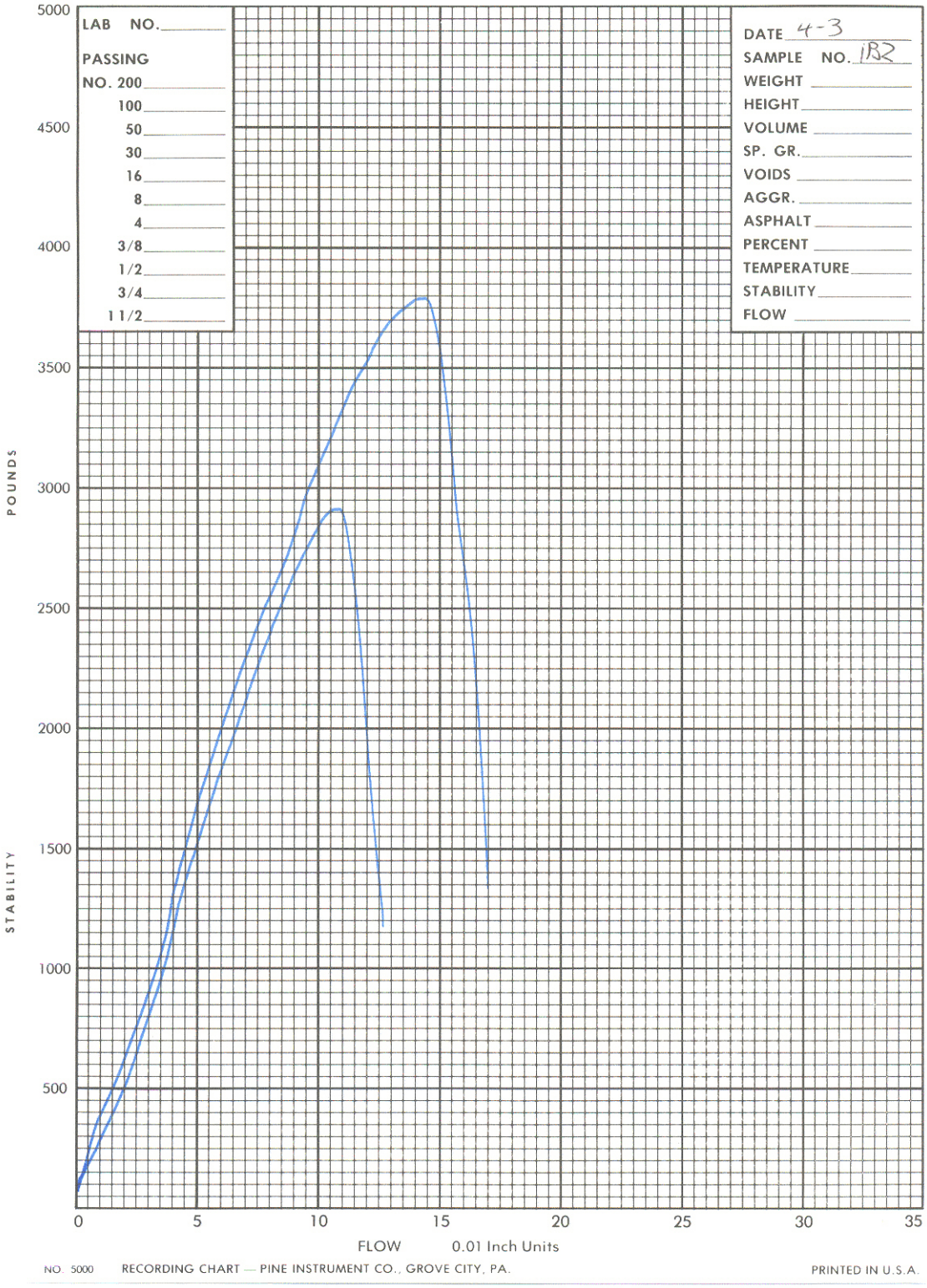

Figure 4.17 Core 1B2 Bond Strength Results. (Note: 10,000 lbs used, not 5,000).

However, this was not the case for the N7 cores. While N8 core load values immediately decreased upon reaching the maximum load, N7 core load values reached the maximum

load and very slowly tapered off. Cores from N7 were able to hold load even after they had reached their maximum shear strength. So, even though the bond strength values were not numerically very different, cores from N7 demonstrated the ability to sustain shear loads near maximum for a longer period of time (Figure 4.18).

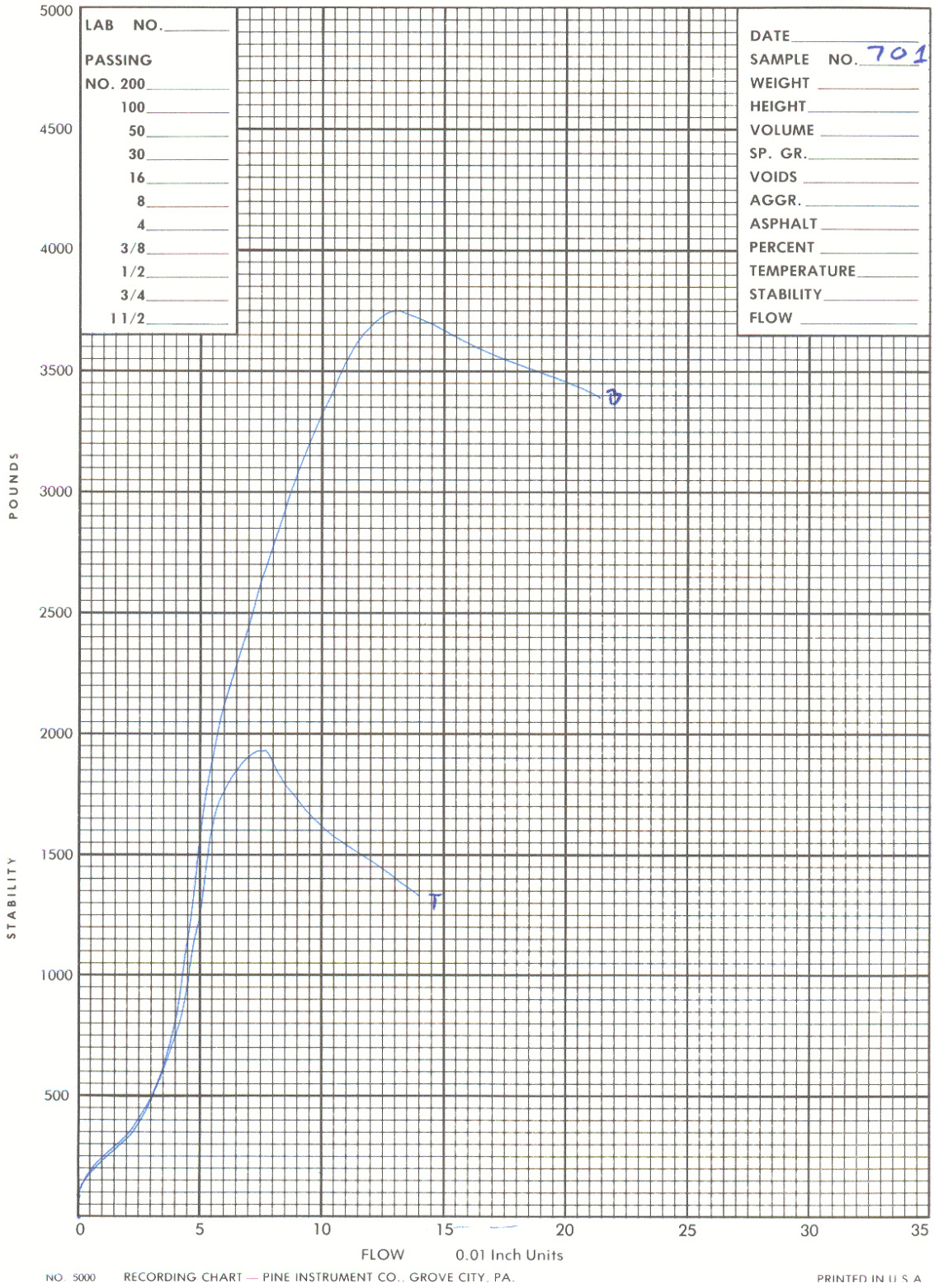

Figure 4.18 Core 7O2 Bond Strength Test Results.

SUMMARY

Very few conclusions could be drawn from the statistical analyses of the actual bond strength values as they were inconsistent throughout the study. However, it can be affirmed that statistically significant differences between the bond strengths of the SMA/HMA interface and that of the HMA/Rich Bottom interface existed.

The most significant differences between core locations occurred in how the samples failed and how they performed after failure. Samples from Trench 2 sheared in multiple locations when being subjected to shear forces at the SMA/HMA interface revealing a light gray colored layer as opposed to the rich black layer expected.. This color change might be due to the grinding of fines due to layer movements. The cores from N7 did not shear along a lift interface, but rather along the aggregate's edges. And even at that point, many of the samples did not physically separate due to the shear.

Perhaps the most revealing bonding information came from a simple visual inspection of the post-failure graphs. N8's cores failed and could no longer hold any load. N7's cores sustained the ability to carry load even after reaching their maximum shear capacity.

CHAPTER 5 - CONCLUSIONS AND RECOMMENDATIONS

SUMMARY

Rich-bottom pavements are designed to increase fatigue resistance at the bottom of an HMA pavement structure through adding an additional 0.5% of asphalt binder to the mixture, thus reducing the amount of air voids in the pavement. While this is the theoretical case, section N8 at the NCAT Test Track, a rich-bottom pavement, exhibited excessive amounts of fatigue cracking despite the additional asphalt. A dynamic strain analysis, physical trench analysis, and a bond strength analysis were conducted in order to determine if the rich-bottom might have been the cause of the accelerated damage. Based upon this investigation, the following conclusions are made:

CONCLUSIONS

1. Both theoretical and dynamic strain support the theory of slippage occurring in section N8. This is seen through the matching of theoretical slippage ratios to the actual dynamic strain ratios measured for slippage occurring at both the SMA/HMA interface and the HMA/rich bottom interface.
2. Cracking began above the rich bottom layer. Strain profiles show that lower strains were seen at the base of the rich bottom layer. This is supported by the crack mapping exercises that showed the rich bottom layer to be mostly free from cracks except for the extreme deterioration condition of Trench 1.
3. Bond strengths were stronger at the bottom of the pavement than at the top of the pavement. Strength values from the Marshall Pine Press and the amount of debonding visually seen at these interfaces support this finding.
4. The cores from N7 had a greater residual strength than those from N8. N7 might have been able to sustain more repetitions of higher shear loading than those in N8. This observation was true for both interfaces (SMA/HMA and HMA/Rich Bottom).
5. The loss of bond is likely the cause of early cracking here. Some states do not use tack coats if layers are constructed on the same day. Tack coats should be used to increase bond strength.

RECOMMENDATIONS

It is recommended that study continues in this area. The effects of cyclical loading on bond strength and its relation to field performance should be investigated further. If a pavement has a strong bond, it is worthless unless the structure is able to withstand multiple loadings as seen with heavy interstate traffic. Bond strength between layers should be studied to help prevent early-age cracking.

Section N8 was not able to validate the usefulness of a rich-bottom layer to resist fatigue cracking due to its debonding problems and consequential failure. Two new structural sections were constructed as part of the 2006-2009 study at the NCAT Test Track to further investigate the rich-bottom concept. These sections were designed by Oklahoma Department of Transportation engineers for lower air voids as opposed to just increasing the asphalt content.

REFERENCES

1. Asphalt Pavement Alliance, "Perpetual Pavements: A Synthesis," APA 101, Asphalt Pavement Alliance, 2002.
2. Harm, E., "Illinois Extended-Life Hot Mix Asphalt Pavements," Transportation Research Circular Number 503, 2001, pp 108-113.
3. Harvey, J., Monismith, C., Horonjeff, R., Bejarano, M., Tsai, B.W. and V. Kannekanti, "Long-Life AC Pavements: A Discussion of Design and Construction Criteria Based on California Experience," International Symposium on Design and Construction of Long Lasting Asphalt Pavements: Proceedings, National Center for Asphalt Technology, 2004, pp 285-333.
4. Huang, Y.H., *Pavement Analysis and Design*, Prentice Hall: New Jersey, 1993.
5. Newcomb, D.E., Buncher, M., and I.J. Huddleston, "Concepts of Perpetual Pavements," Transportation Research Circular, Number 503, 2001, pp 4-11.
6. Priest, A.L. and D.H. Timm, "A Full Scale Structural Pavement Structural Study for Mechanistic-Empirical Pavement Design," Journal of the Association of Asphalt Paving Technologists, Vol. 74, 2005, pp. 519-556.
7. Priest, A.L., "Calibration of Fatigue Transfer Functions for Mechanistic-Empirical Flexible Pavement Design," M.S. Thesis, Auburn University, 2005.
8. St. Martin, J., Harvey, J.T., Long, F., Lee, E., Monismith, C., and K. Herritt, "Long-Life Rehabilitation Design and Construction: I-710 Freeway, Long Beach, California," Transportation Research Circular, Number 503, 2001, pp 50-65.
9. Timm, D.H. and A.L. Priest, "Material Properties of the 2003 NCAT Test Track Structural Study," NCAT 06-01, National Center for Asphalt Technology, 2006.
10. Timm, D.H., Priest, A.L. and McEwen, T.V., "Design and Instrumentation of the Structural Pavement Experiment at the NCAT Test Track," NCAT 04-01, National Center for Asphalt Technology, 2004.
11. West, R.C., Zhang, J. and J. Moore, "Evaluation of Bond Strength Between Pavement Layers," NCAT 05-08, National Center for Asphalt Technology, 2005.

APPENDIX A – BOND STRENGTH TESTING

Table A.1: Bond Strength Test Results

Trench	Location	Position	SMA/HMA Bond Strength, psi	HMA/Rich Bottom Bond Strength, psi
1	A	1	141.47	280.11
1	A	2	143.24	298.86
1	A	3	114.95	309.47
1	A	4	146.78	333.16
1	A	5	239.09	284.36
1	B	1	177.90	280.11
1	B	2	205.84	267.73
1	B	3	118.84	287.19
1	B	4	145.01	261.72
1	B	5	97.26	234.13
2	I	1	129.09	290.72
2	I	2	149.25	281.53
2	I	3	130.86	293.91
2	I	4	121.31	281.17
2	I	5	101.86	284.36
2	O	1	113.18	221.05
2	O	2	104.69	235.20
2	O	3	25.46	237.67
2	O	4	148.54	268.80
2	O	5	113.88	252.88
3	I	1	327.15	281.17
3	I	2	258.89	312.30
3	I	3	150.67	302.39
3	I	4	290.02	298.86
3	I	5	282.59	302.39
3	O	1	126.26	205.13
3	O	2	165.17	273.04
3	O	3	150.31	317.60
3	O	4	182.50	300.63
3	O	5	202.30	290.72
7	I	1	153.85	269.50
7	I	2	149.25	295.32
7	I	3	153.85	282.94
7	I	4	158.45	276.93
7	I	5	148.54	274.10
7	O	1	136.17	265.26
7	O	2	130.15	308.41
7	O	3	104.33	270.56
7	O	4	158.45	263.49
7	O	5	114.95	297.09

Note: I = inside wheelpath, O = outside wheelpath, A = After trench, B = Before trench

APPENDIX B – SHEAR TESTING DATA PLOTS

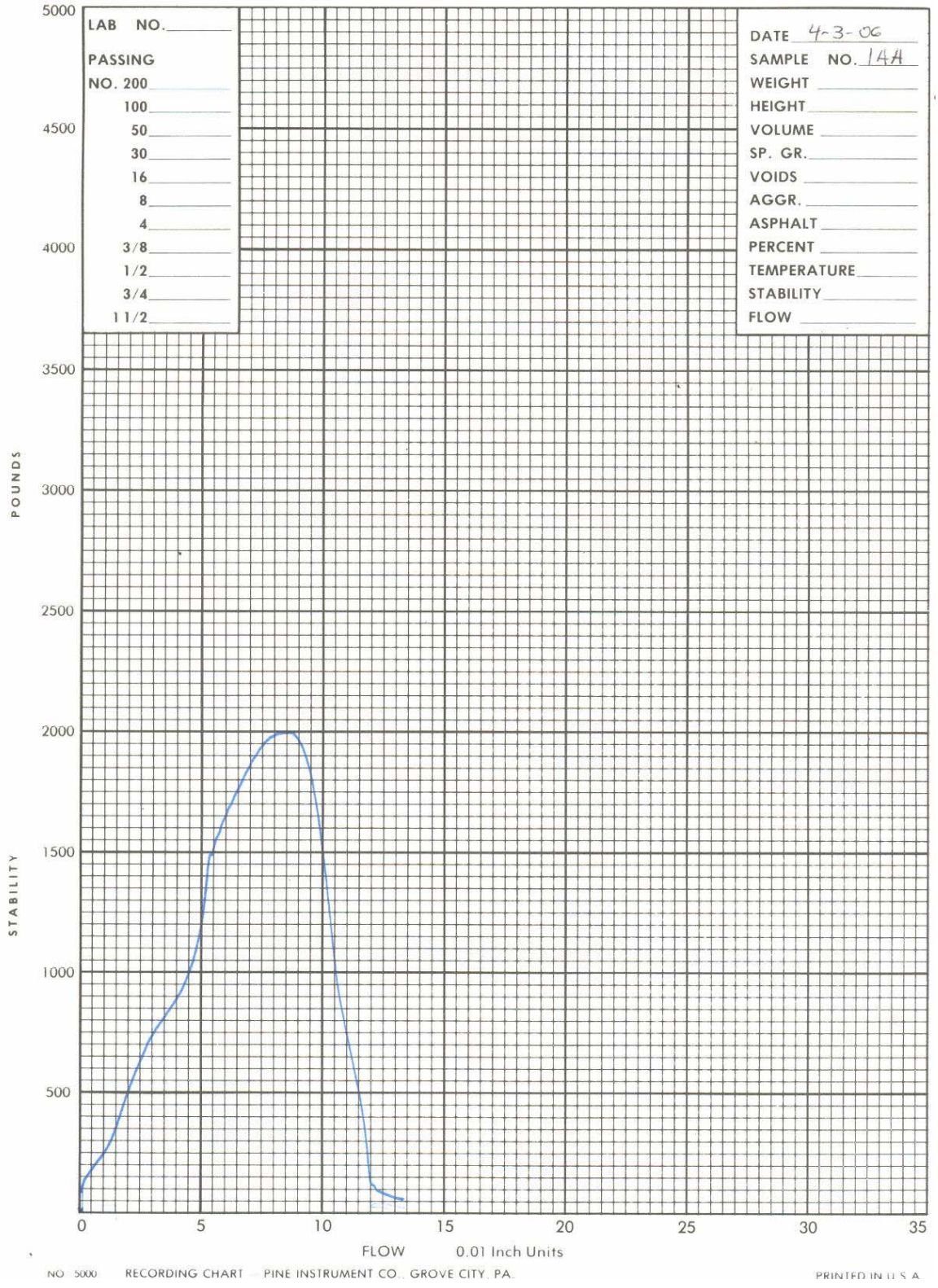

Figure B.1 Enlarged Marshall Stability Chart for Core 1A1 Top.

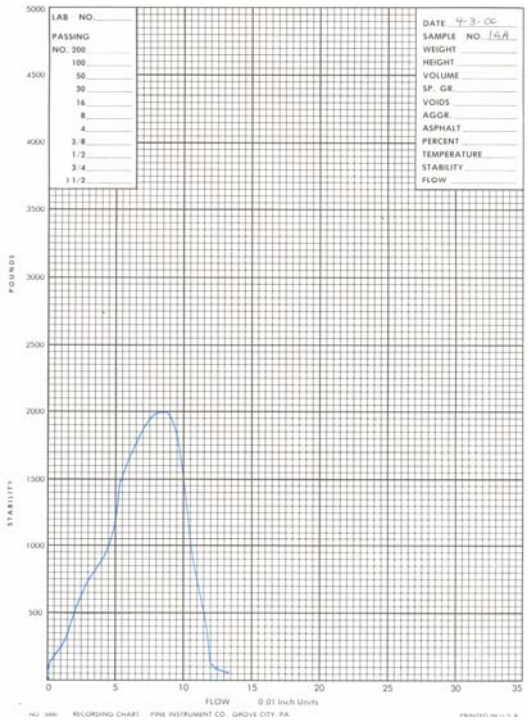

Figure B.2: Core 1A1 Top

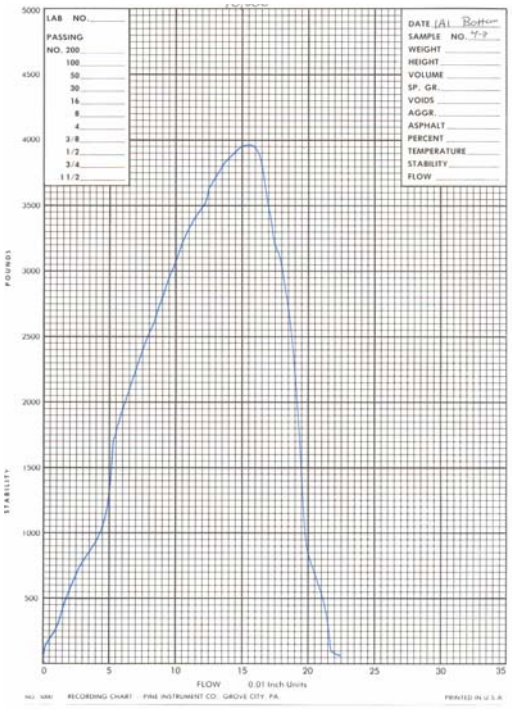

Figure B.3: Core 1A1 Bottom

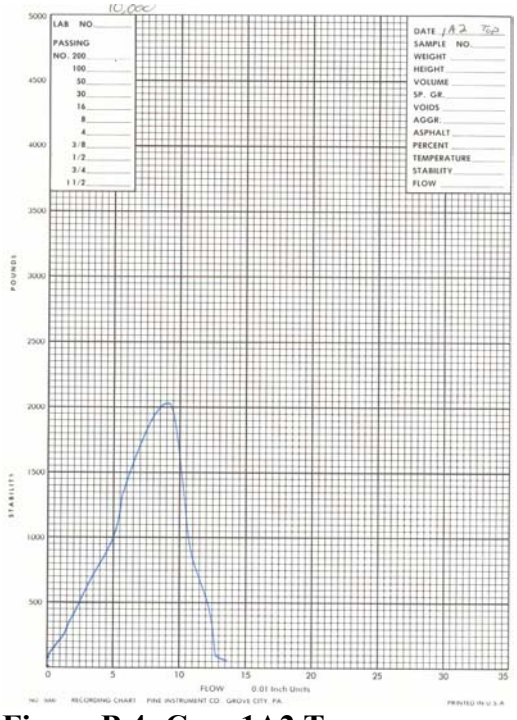

Figure B.4: Core 1A2 Top

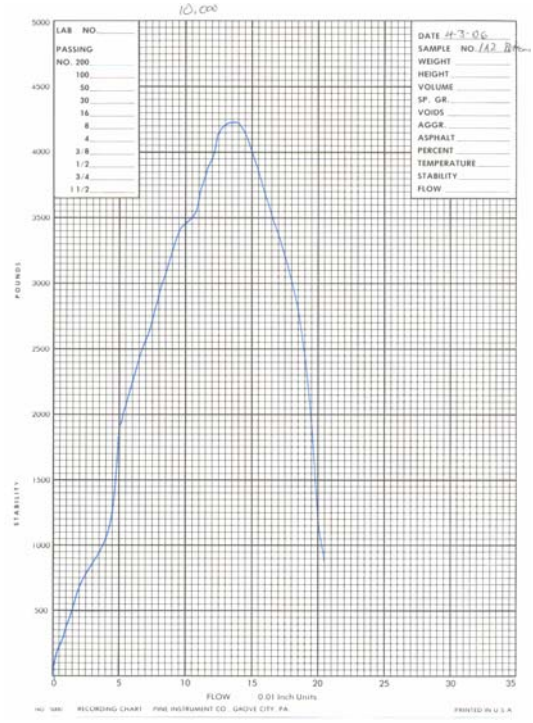

Figure B.5: Core 1A2 Bottom

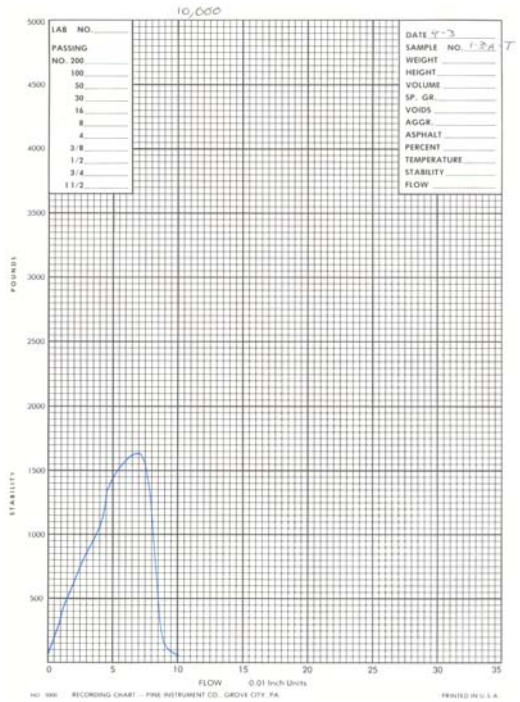

Figure B.6 Core 1A3 Top

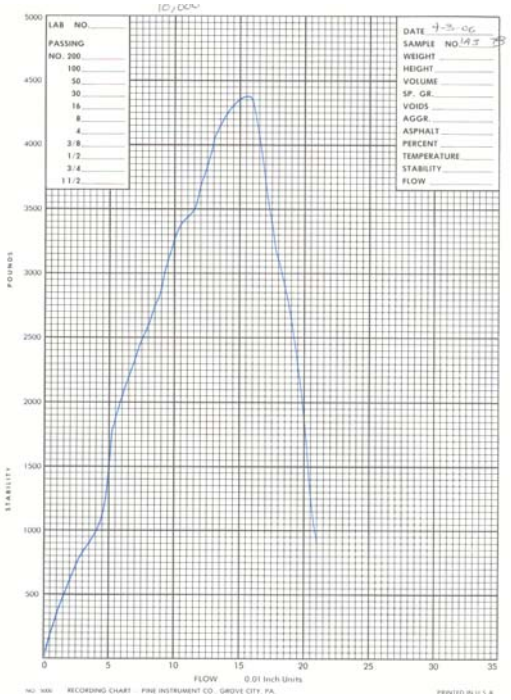

Figure B.7 Core 1A3 Bottom

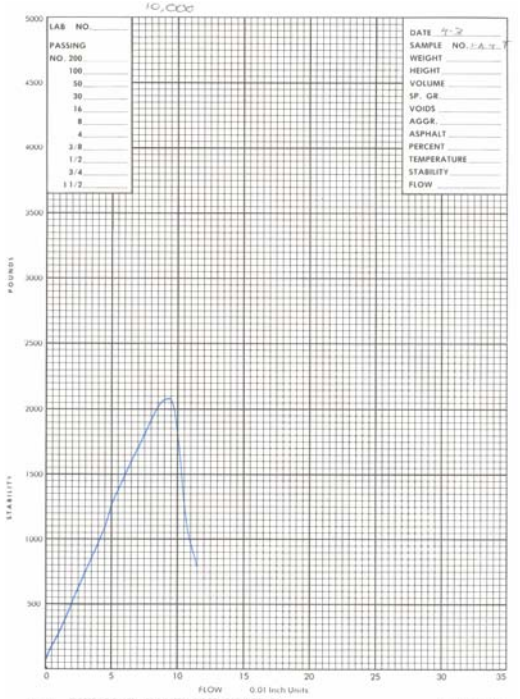

Figure B.8 Core 1A4 Top

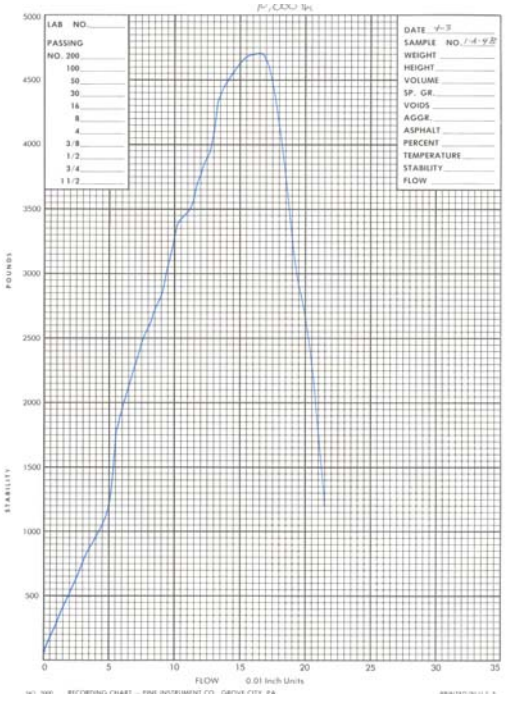

Figure B.9 Core 1A4 Bottom

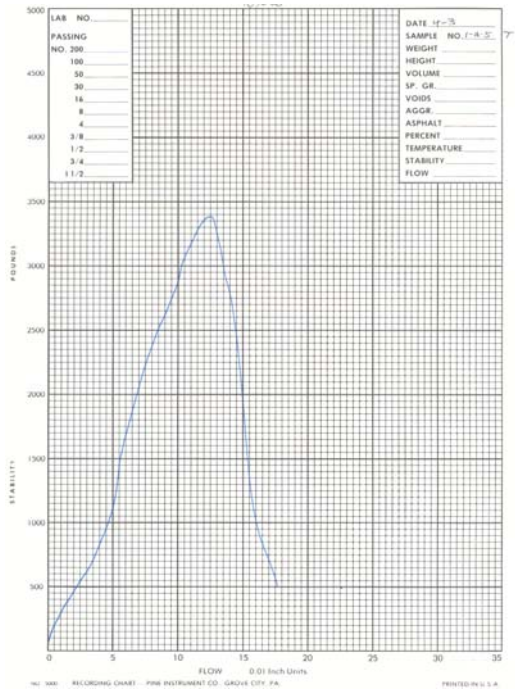

Figure B.10 Core 1A5 Top

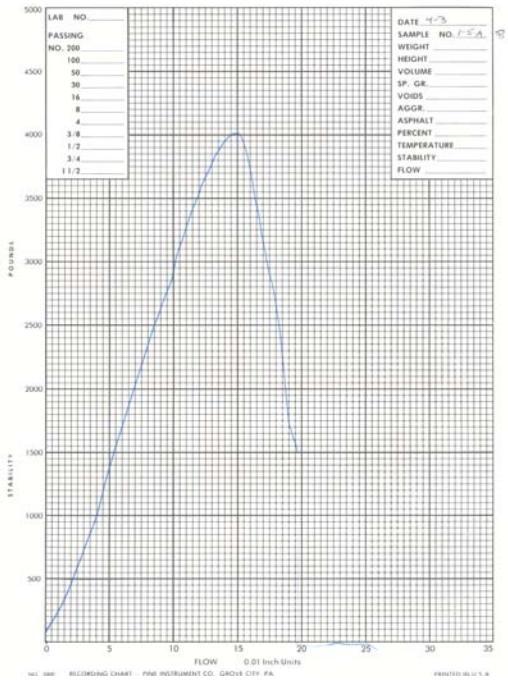

Figure B.11 Core 1A5 Bottom

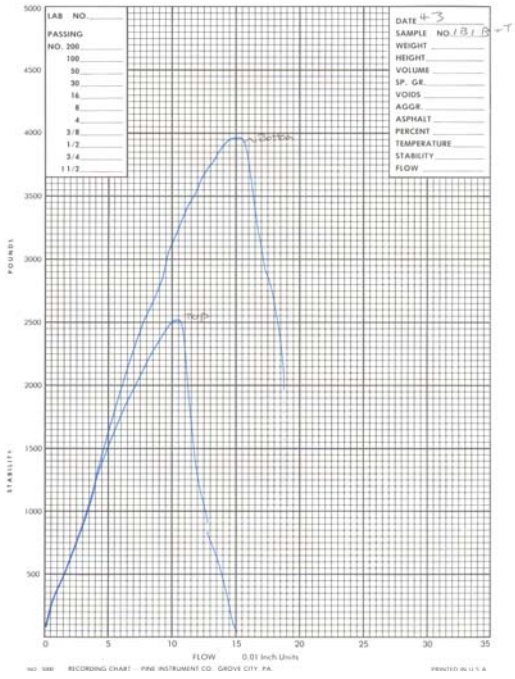

Figure B.12 Core 1B1

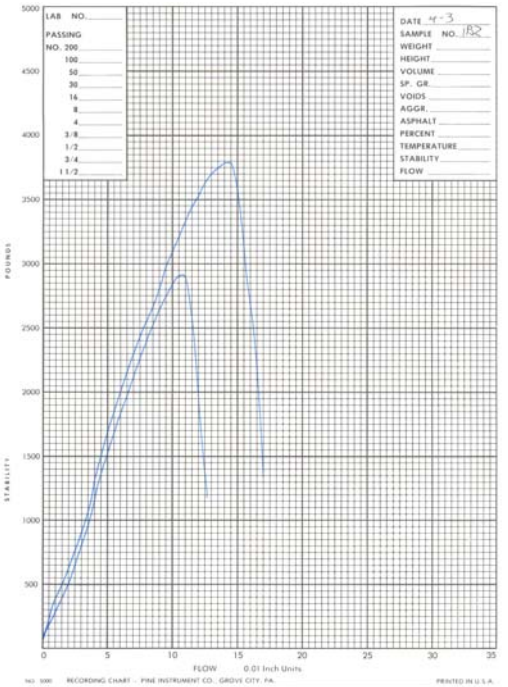

Figure B.13 Core 1B2

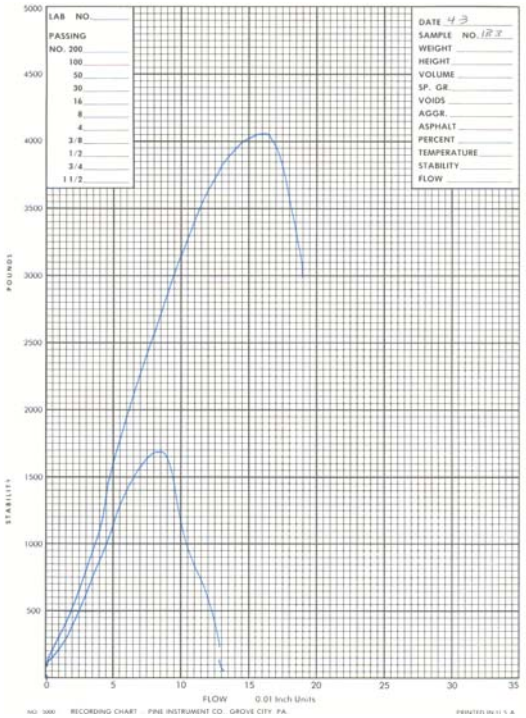

Figure B.14 Core 1B3

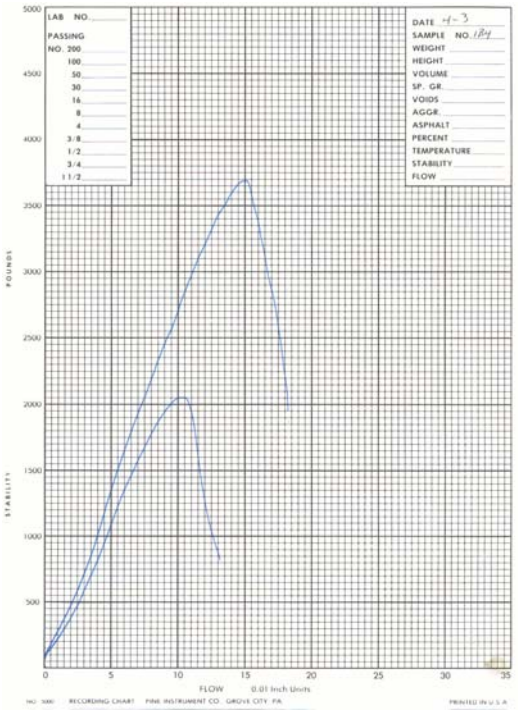

Figure B.15 1B4

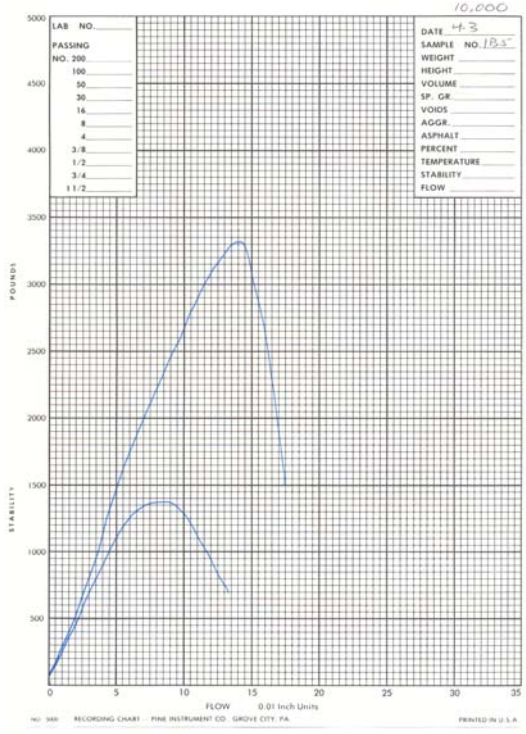

Figure B.16 Core 1B5

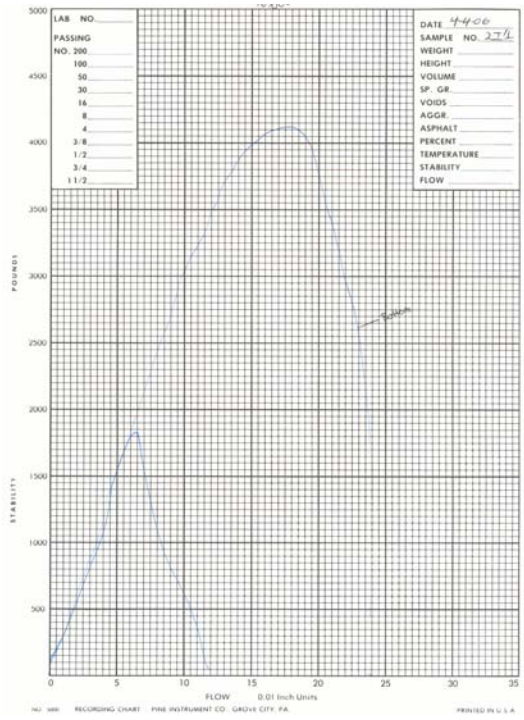

Figure B.17 Core 2I1

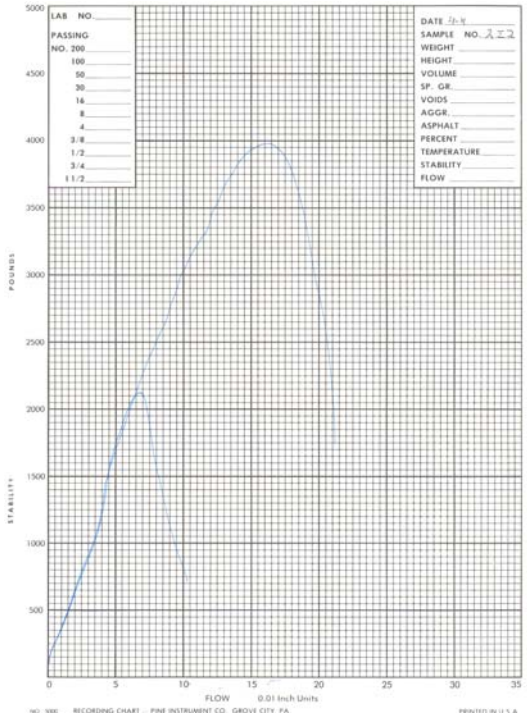

Figure B.18 Core 2I2

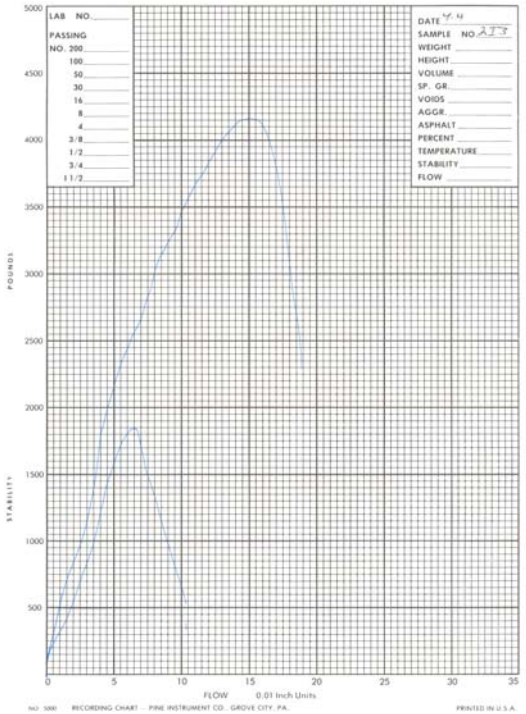

Figure B.19 Core 2I3

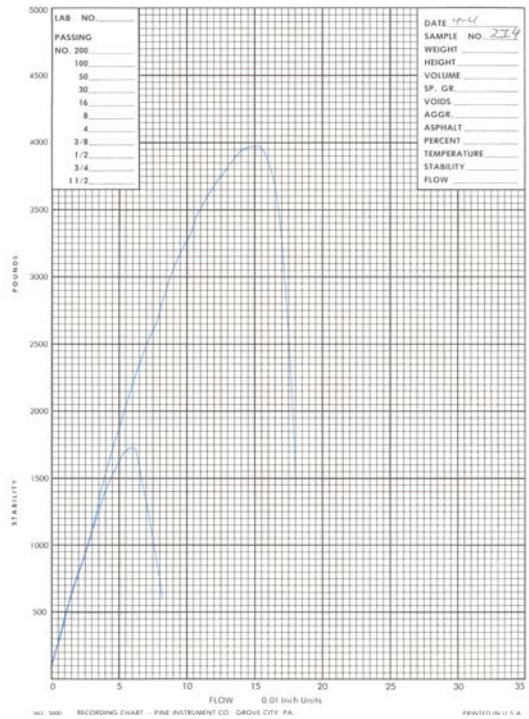

Figure B.20 Core 2I4

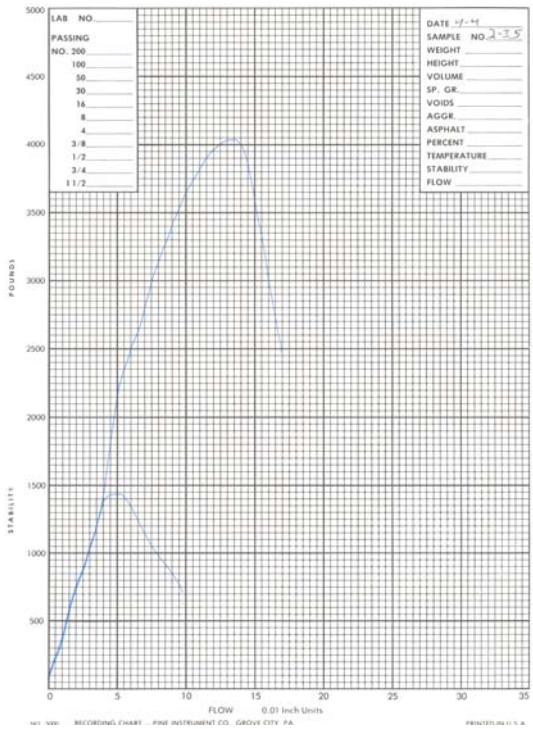

Figure B.21 Core 2I5

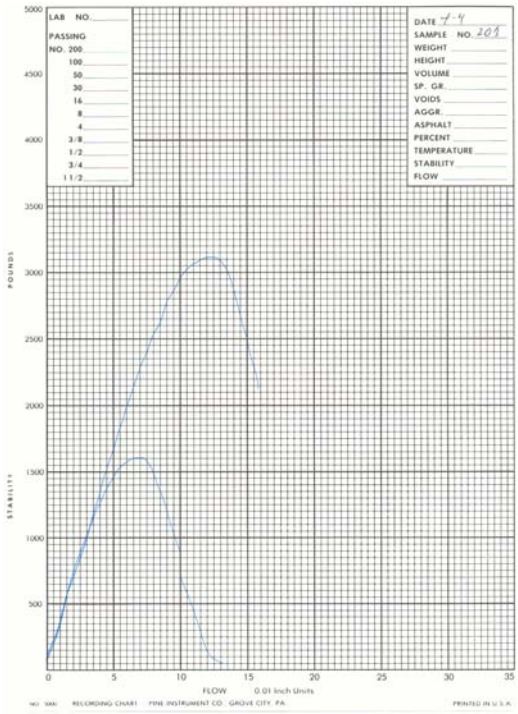

Figure B.22 Core 2O1

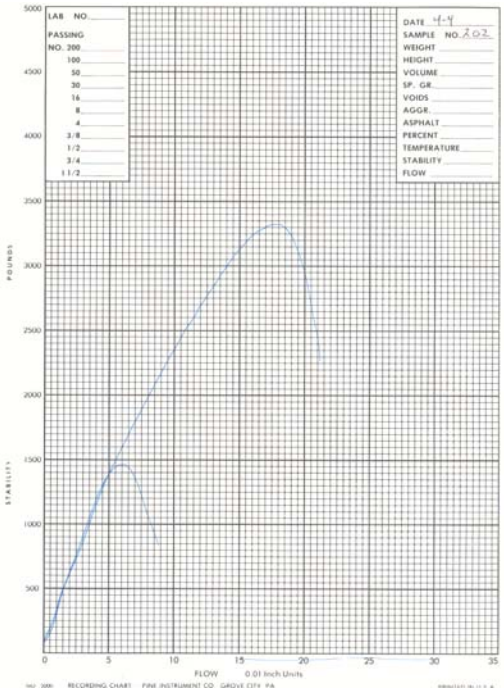

Figure B.23 Core 2O2

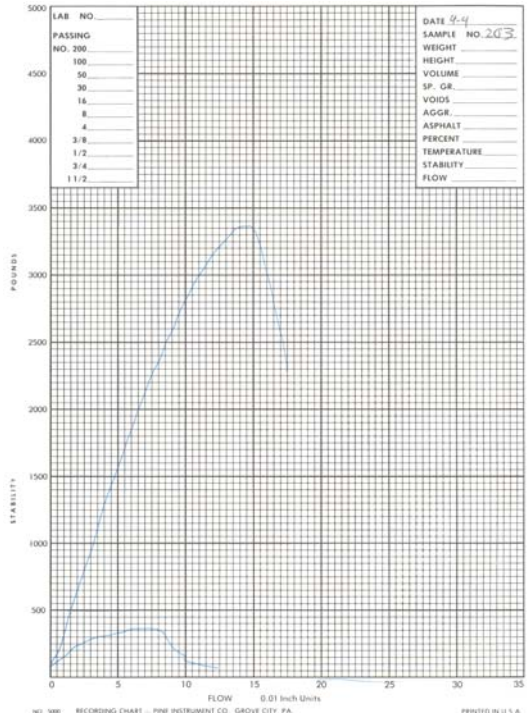

Figure B.24 Core 2O3

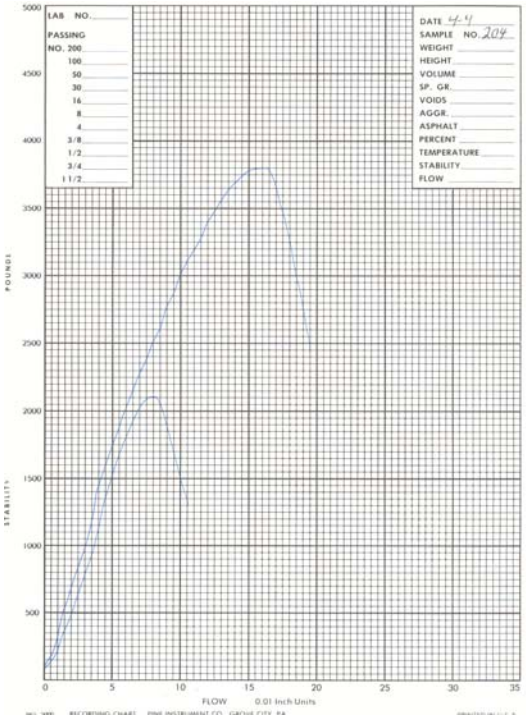

Figure B.25 Core 2O4

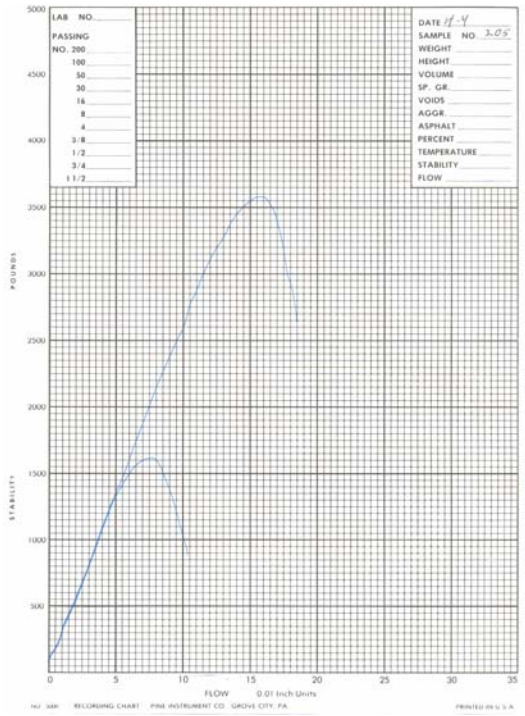

Figure B.26 Core 2O5

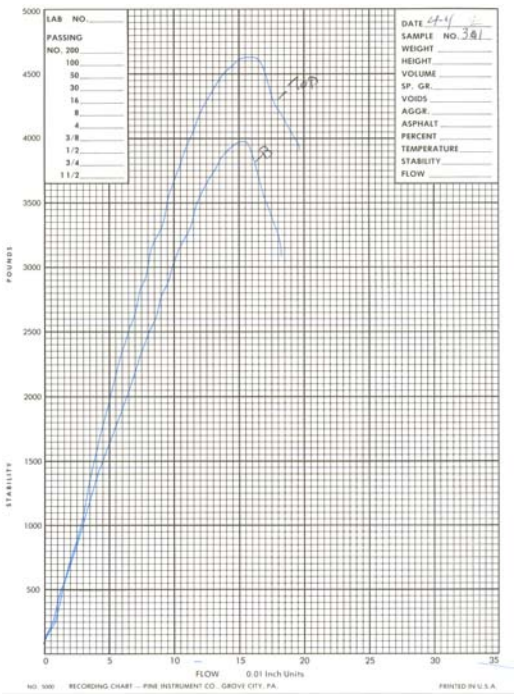

Figure B.27 Core 3I1

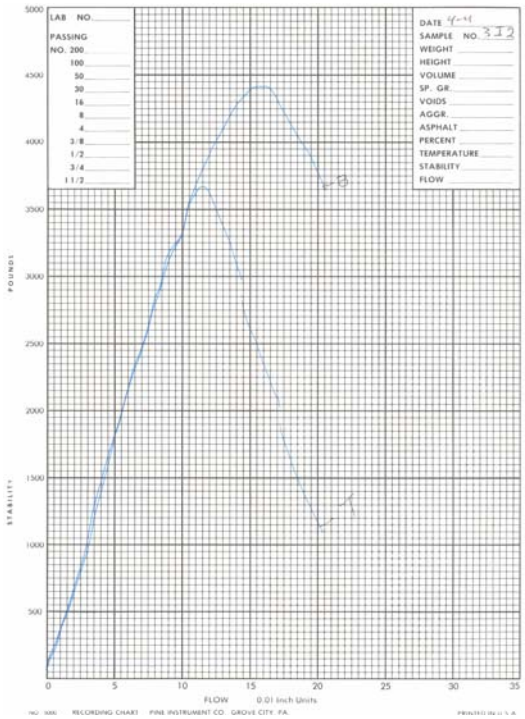

Figure B.28 Core 3I2

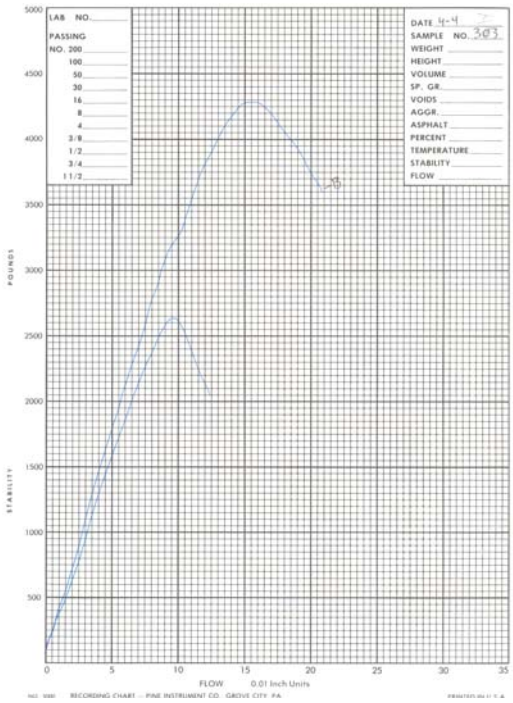

Figure B.29 Core 3I3

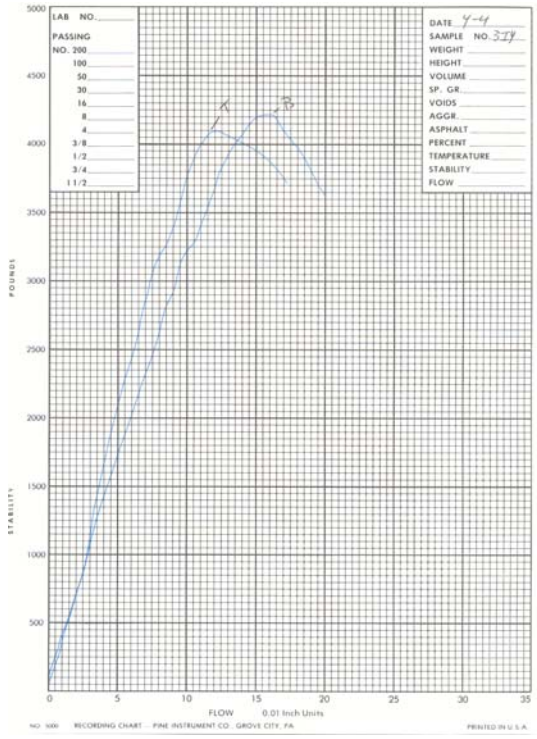

Figure B.30 Core 3I4

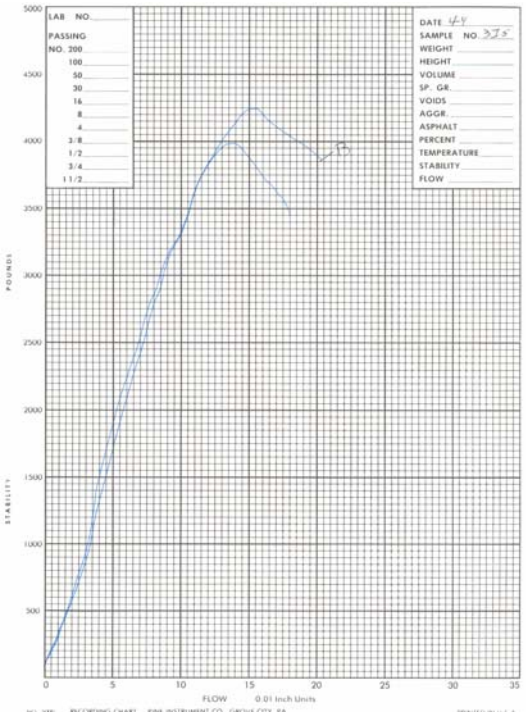

Figure B.31 Core 3I5

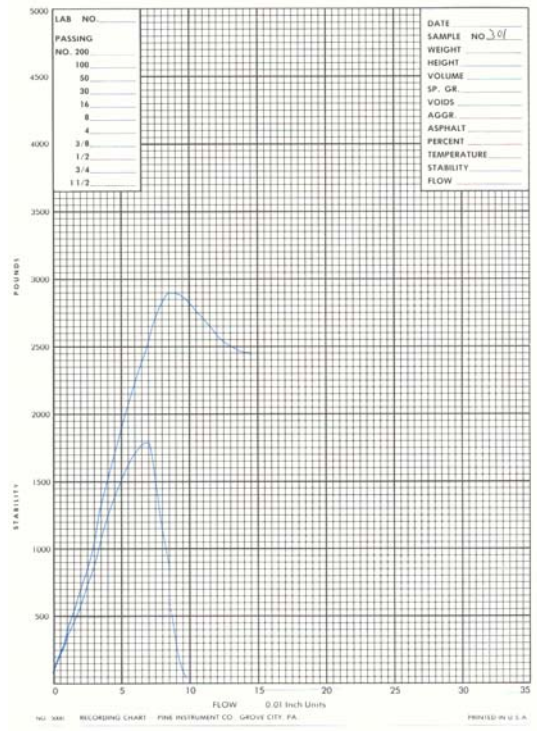

Figure B.32 Core 3O1

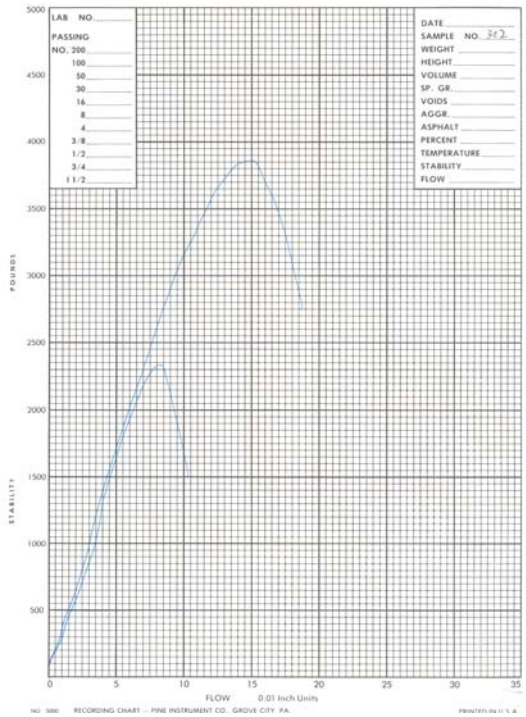

Figure B.33 Core 3O2

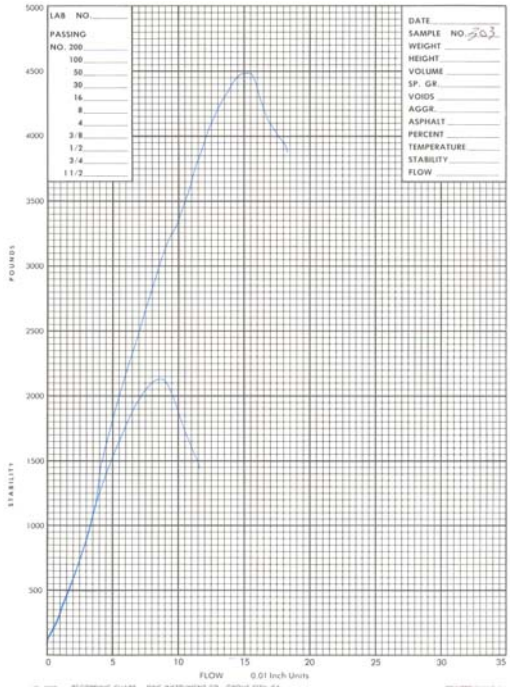

Figure B.34 Core 3O3

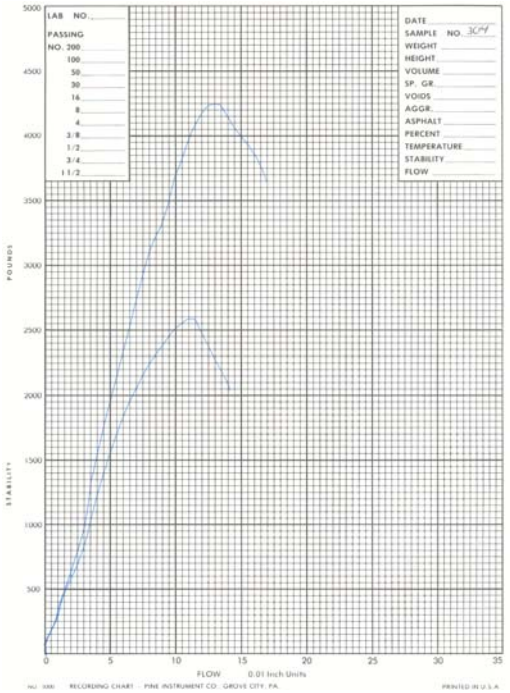

Figure B.35 Core 3O4

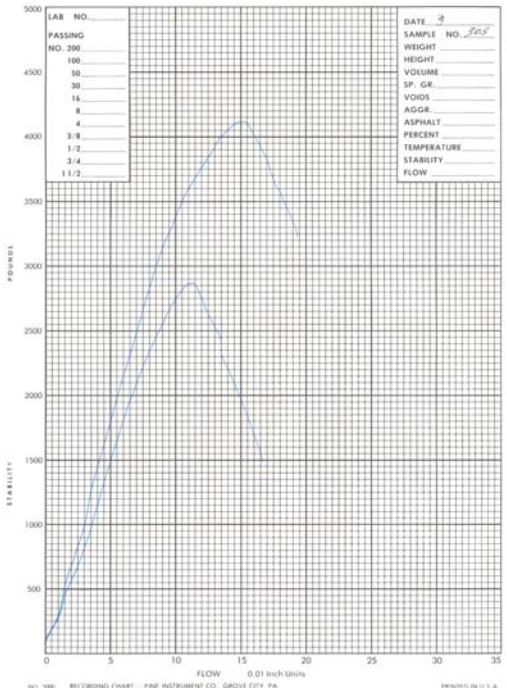

Figure B.36 Core 3O5

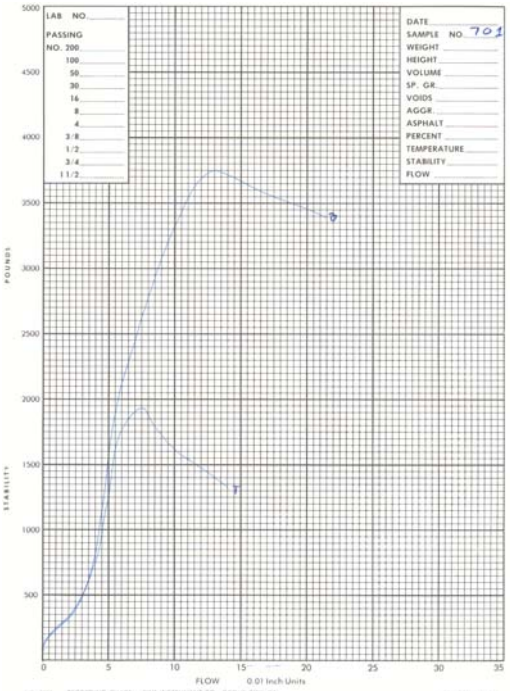

Figure B.37 Core7O1

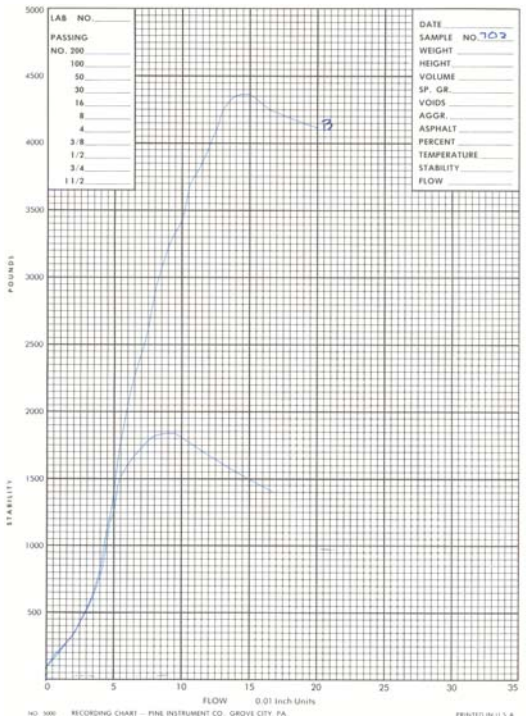

Figure B.38 Core 7O2

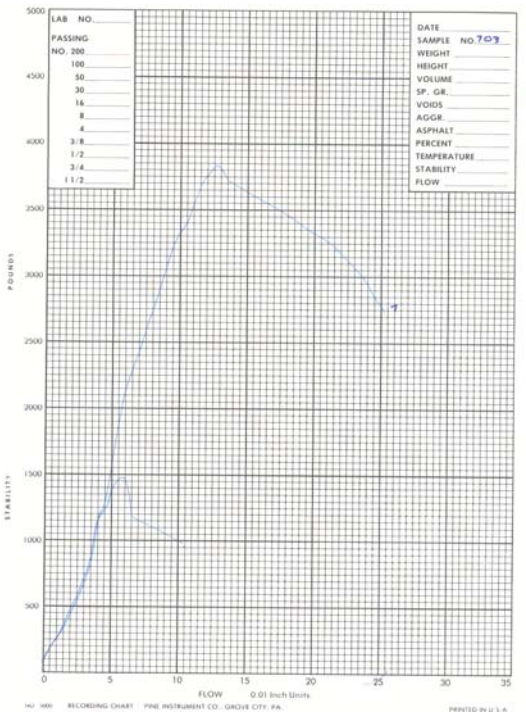

Figure B.39 Core 7O3

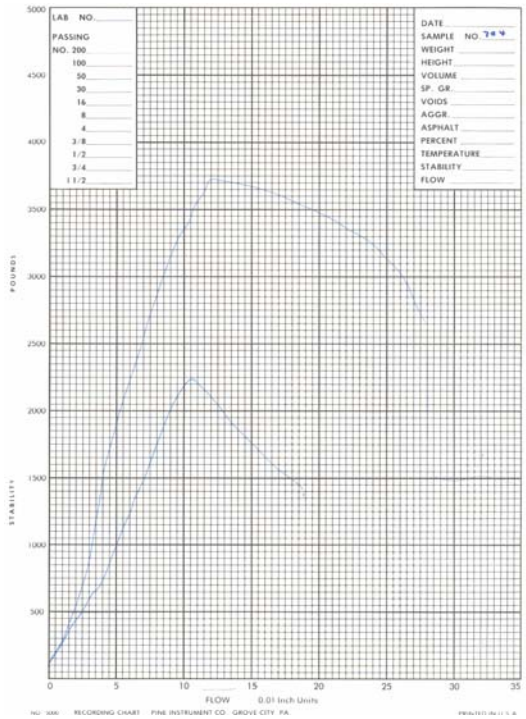

Figure B.40 Core 7O4

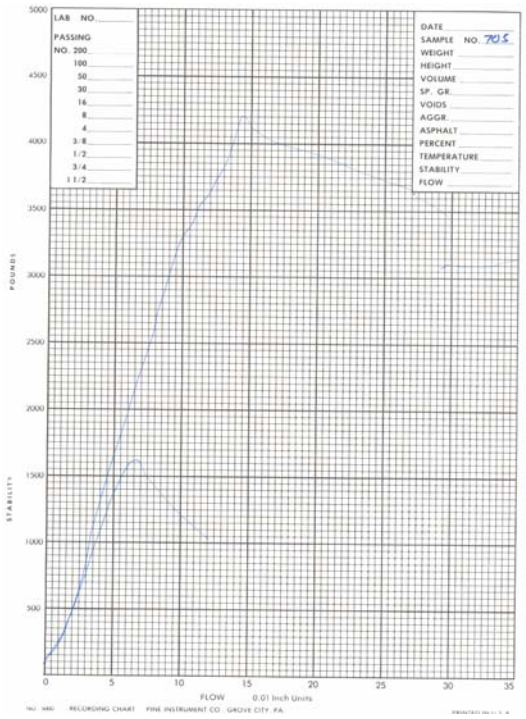

Figure B.41 Core 7O5

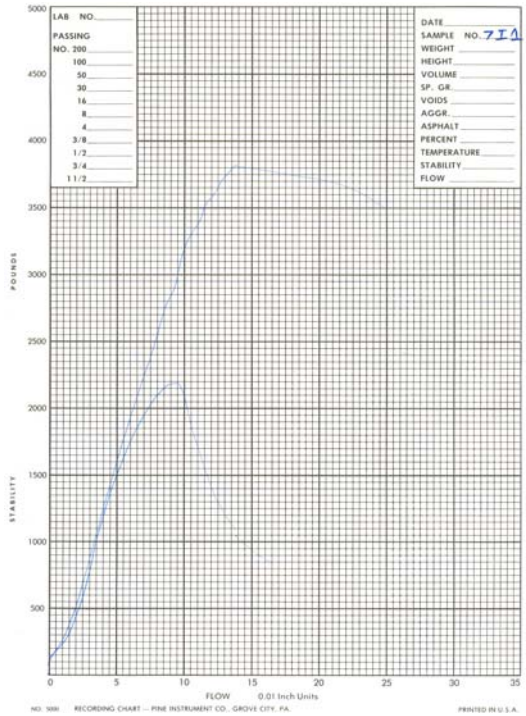

Figure B.42 Core 7I1

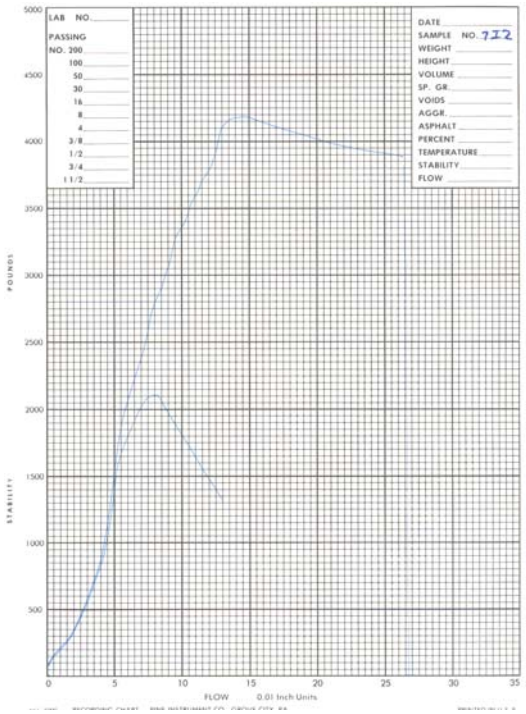

Figure B.43 Core 7I2

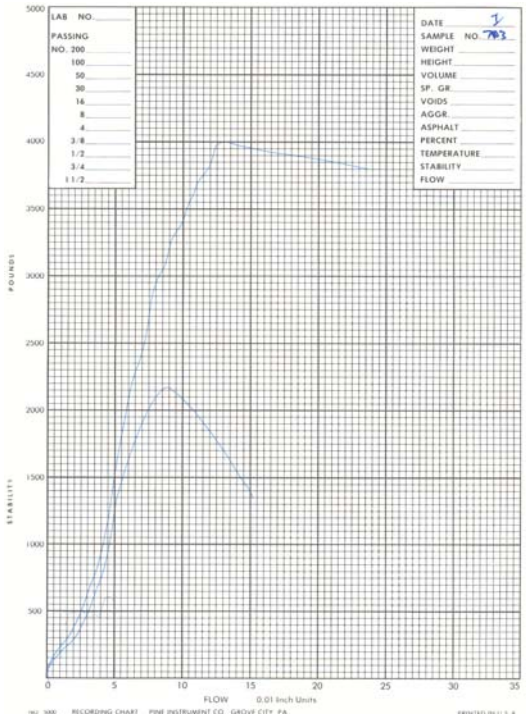

Figure B.44 Core 7I3

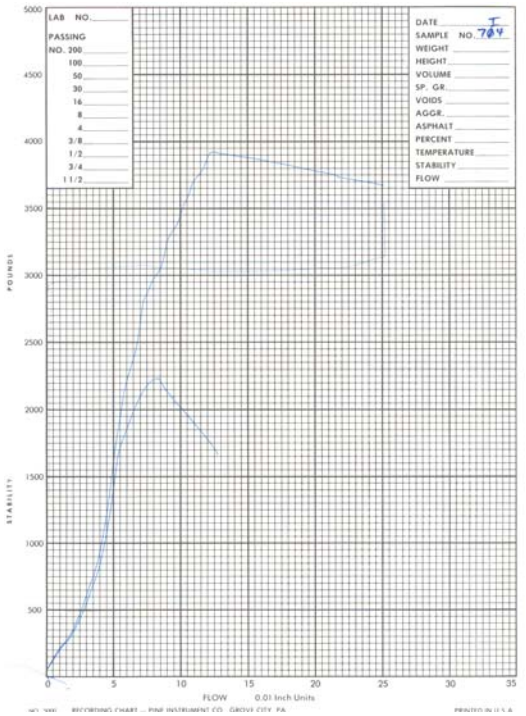

Figure B.45 Core 7I4

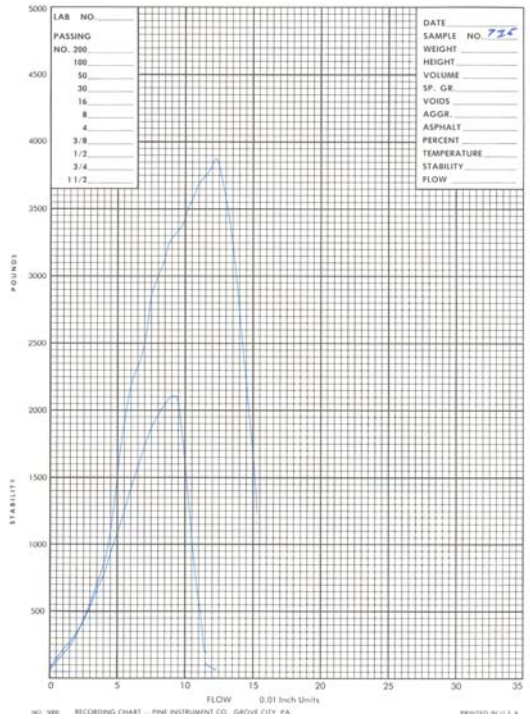

Figure B.46 Core 7I5